

Sources of Errors in Rainfall Measurements by Polarimetric Radar: Variability of Drop Size Distributions, Observational Noise, and Variation of Relationships between R and Polarimetric Parameters

GYUWON LEE

J. S. Marshall Radar Observatory, Department of Atmospheric and Oceanic Sciences, McGill University, Montreal, Quebec, Canada

(Manuscript received 8 December 2004, in final form 24 December 2005)

ABSTRACT

Using a set of long-term disdrometric data and of actual radar measurements from the McGill S-band operational polarimetric radar, several sources of errors in rain measurement with polarimetric radar are explored in order to investigate their relative importance and the feasibility of a polarimetric technique for estimating R in the context of the McGill S-band operational radar that performs a full volume scan of 24 plan position indicators (PPIs) every 5 min. The sources of errors considered are the variability of drop size distributions (DSDs), observational noise, and systematic variation of the relationships between R and polarimetric parameters at different climate regimes.

Additional polarimetric parameters dramatically reduce the effect of the DSD variability on rain estimates by radar. The effectiveness of various multiparameter relationships is investigated. The relationships from the literature that are derived from the DSD model and measured DSDs at a different climate regime differ from those derived from the disdrometric dataset herein. An application of these relationships to the Montreal dataset results in a *bias* (about 10%–20%) and *the significant random error* resulting from the DSD variability. These errors should be eliminated by using a relationship suitable for the local climate.

Assuming a measurement noise as expected from a slow scanning polarimetric radar [~ 1 rotation per minute (rpm)] and a 10-min smoothing, the $R - (Z_h, Z_{DR})$ relationship outperforms the conventional $R - Z_h$ because of the combined effect of the DSD variability and measurement errors. In addition, the marginal measurement noise that is required to have the same accuracy of $R - Z_h$ and $R - (Z_h, Z_{DR})$ algorithms is obtained as a function of temporal smoothing. The quantified measurement noise of the McGill S-band fast scanning operational radar (~ 6 rpm) is significantly larger than that of a slow scanning radar, implying that a temporal averaging of Z_{DR} of 1 h is needed to achieve some gain with $R - (Z_h, Z_{DR})$.

1. Introduction

Advances in radar technology and the development of polarimetric measurements have opened the way for new techniques of radar rain estimation as well as the possibility of target identification of hydrometers (Sachidananda and Zrnic 1987; Chandrasekar and Bringi 1988; Chandrasekar et al. 1990; Ryzhkov and Zrnic 1995, 1998; Vivekanandan et al. 1999; Liu and Chandrasekar 2000). Target identification aids the data quality control, that is, permits the elimination of ground echoes (GEs) and of the nonprecipitation echoes from birds or insects. Furthermore, knowledge of the proper

phases of precipitation based on target identification is an essential element in radar data assimilation in an effort to improve quantitative precipitation forecasting.

Potential improvement in rain estimation by polarimetric parameters (Z_h and Z_{DR}) was suggested by Seliga and Bringi (1976). They emphasized that the differential reflectivity Z_{DR} is a measure of mean drop size that is independent of the number concentration and is related to the slope parameter λ of the exponential drop size distribution (DSD) [$N(D) = N_0 e^{-\lambda D}$]. [Note that N_0 is not fixed as in the Marshall and Palmer (1948) DSDs.] Provided that the mean drop size is known, the intercept parameter N_0 can be derived from Z_h . Subsequently, R can be derived from the mean drop size and N_0 . In addition, the specific differential phase shift K_{DP} is related to R with a power law in which the exponent is close to 1 (e.g., $R = 40.8 K_{DP}^{0.850}$), whereas the exponent of the R – Z relationship is much smaller than

Corresponding author address: Dr. GyuWon Lee, J. S. Marshall Radar Observatory, McGill University, P.O. Box 198, Macdonald Campus, Ste-Anne de Bellevue QC H9X 3V9, Canada.
E-mail: gyuwon.lee@mail.mcgill.ca

1 (i.e., $R = 0.0234Z_h^{0.683}$). Here, K_{DP} is defined as being one way. Here, Z_h can be approximated by the sixth moment of the DSDs and R by the 3.67th moment. Consequently, the estimation of R with an R - K_{DP} relationship is less affected by the physical variability of DSDs than is the case with the R - Z_h relationship. Therefore, the main advantage of estimating R with polarimetric parameters is related to the reduction of the *physical* variability of DSDs.

However, observed radar parameters are subject to the *statistical* noise resulting from the random positions and velocities of raindrops within a sampling volume (Doviak and Zrníc 1993). The conventional rain estimation algorithms with the horizontal or vertical reflectivities, Z_h or Z_v , are relatively less affected by this statistical noise. A *relative* statistical noise in Z_{DR} and K_{DP} depends on the correlation of signals in horizontal and vertical channels. As the correlation increases, the relative statistical noise decreases. When the polarimetric signature is strong as in heavy rain, the statistical noise is relatively small. Therefore, a comparison of the uncertainty in R resulting from the statistical noise and physical variability is essential in order to provide a guideline in radar rain estimation and to investigate the accuracy of polarimetric techniques.

As in the rain estimation with conventional R - Z relationships, the application of polarimetric techniques to radar hydrology requires relationships between the polarimetric parameters and rainfall rate. These relationships are usually calculated by assuming an exponential or gamma drop size distribution with a common range of DSD parameters (Illingworth and Blackman 2002, and references therein). The common range of gamma DSD parameters (N_0 , λ , and μ) is originally obtained by comparing the exponent and coefficient of 69 R - Z relationships in Battan (1973) with the derived relationship from the gamma DSD model (Ulbrich 1983). However, those R - Z relationships depend on the regression method by which they were derived and on the different instruments used in each case (Ciach and Krajewski 1999; Uijlenhoet 1999; Campos and Zawadzki 2000; Ciach et al. 2000; Salles and Creutin 2003; Lee and Zawadzki 2005a). Hence, the obtained common range is quite questionable. It is also widely known that the gamma DSD cannot explain the multimodal distribution and S-shaped DSDs (i.e., of a relative lack of medium-sized drops and larger number of small and big drops: Fig. 7 of Sauvageot and Lacaux 1995; Fig. 10 of Uijlenhoet et al. 2003; Fig. 4.7 of Lee 2003; Fig. 1 of Montero-Martinez and Garcia-Garcia 2004; Fig. 6 of Zawadzki and Lee 2004), which are frequently observed with modern disdrometers. To overcome this limitation, Auf der Maur (2001) proposes a

generalized gamma as an alternative to better describe the real shape of DSDs. The specific DSD model has definite advantages in the simple representation of DSDs and in the parameterization for numerical models. However, when a large database of reliable disdrometric data is available, error statistics and relationships in rain estimation can be directly obtained from actual disdrometric data rather than from any specific DSD model. It will thus be possible to fully represent possible physical variability at a climate regime without adding an unnecessary model error. In addition, because the DSD variability depends on climatology, that is, the geographic component, its effect on rain estimation is better studied using actual local DSD variability.

The purpose of this paper is to explore the following issues:

- (i) a detailed error analysis in R estimation resulting from the DSD variability,
- (ii) a comparison of the relationships used in R estimation derived from the specific model DSDs and from observed DSDs, and
- (iii) the feasibility of polarimetric techniques in R estimation by investigating errors resulting from the DSD variability and measurement noise.

The DSD dataset used is limited to a single climate region, Montreal, Quebec, Canada. The scanning strategy of a dual-polarization radar is based on the McGill S-band radar, which maximizes the volumetric surveillance. Thus, all conclusions should be interpreted in the context of the McGill S-band radar and the Montreal environment. In section 2, we describe the disdrometric and radar data used in this paper, and the expected errors in R with the various combinations of polarimetric parameters are shown in section 3. The efficiency of various relationships in the reduction of the DSD variability is also discussed. In section 4, our derived relationships between R and polarimetric parameters are compared with those from the literature. From this comparison, we quantify the systematic variation of the relationships at different climate regimes. Error propagation in R resulting from the DSD variability and measurement errors is shown in section 5, and the conclusions follow.

2. Data used

a. Disdrometric data

A large disdrometric dataset has been obtained from the precipitation occurrence sensing system (POSS; developed by Atmospheric Environment Canada) that operated for 5 yr (1994, 1997–2000) in Montreal. The

detailed description on POSS is given in Sheppard (1990). POSS is a small continuous wave (CW) X-band bistatic radar and measures the average Doppler spectrum every minute on the ground and converts it into a drop size distribution. The number of diameter bins is 34 from 0.34 to 5.4 mm. The diameter intervals (dD) increase with diameter (e.g., $dD = 0.05$ mm at $D = 0.34$ mm and $dD = 1.84$ mm at $D = 5.4$ mm). The number density at $D = 5.4$ mm includes all of the number of drops larger than this diameter. POSS has been carefully calibrated by measuring a precise beam pattern and by simulations, and furthermore was widely validated with other disdrometers and rain gauges (Sheppard and Joe 1994; Campos and Zawadzki 2000). The retrieval algorithm produces an overestimation of the number density at the smallest size ($D = 0.34$ mm) and a broadening of retrieved DSDs (Sheppard 1990). The uncertainty that is related to the DSD retrieval algorithm and undersampling effect is quantified by a Monte Carlo simulation and has been shown to be less than 0.5 dB for R and 1 dB for Z (Sheppard 2006). A similar uncertainty is also quantified with two collocated POSSs (see appendix A).

The sampling volume is three orders of magnitude larger than that of other disdrometers so that undersampling is a second-order problem in POSS (see Lee and Zawadzki 2005a appendix). Most conventional disdrometers have difficulty in measuring big drops because of the small sampling volume. Their measurements are sometimes truncated at $D = 3$ mm even for $R \sim 6$ mm h⁻¹. This shortcoming could prevent the use of disdrometric data for the derivation of polarimetric parameters, especially Z_{DR} . However, because of the large sampling volume, the bigger drops are well measured with POSS (see the comparison of various disdrometers with POSS in Figs. 6–9 of Sheppard and Joe 1994). The research by Miriovsky et al. (2004) shows the underestimation of bigger drops by POSS although rain accumulation from POSS agrees well with rain gauge measurements. It should be noted that in their research 1) four disdrometers are not collocated and 2) 34-bin POSS DSDs are linearly interpolated to 20 Joss-Waldvogel disdrometer (JWD) bins instead of using the original measured DSDs. Our comparison of the collocated JWD and POSS shows that the JWD systematically underestimates bigger drops, resulting into a systematic underestimation of Z (appendix A). However, the large sampling volume has a trade-off. Strong horizontal winds broaden the Doppler power spectra, distorting the distribution. Small and big drops are overestimated because of strong winds, yielding a concave distribution. However, this effect is minimal with hori-

zontal winds < 5 m s⁻¹ (see Fig. 3 of Sheppard and Joe 1994). However, the effects of vertical wind are more significant than those of horizontal winds. The vertical winds directly change the Doppler velocities and hence the diameters, toward smaller values for updraft and larger values for downdraft. An underestimation in R of 20% (overestimation of 30%) can be reached with a $+0.5$ m s⁻¹ downward (-0.5 m s⁻¹ upward) motion (Fig. 3 of Sheppard and Joe 1994). Because POSS measurements are obtained at the ground and more than two-thirds of the cases are stratiform, we assume that the effect of vertical wind should be not significant.

Our dataset is composed of 20 400 one-minute DSDs and includes a variety of rain situations, such as long-lasting stratiform rain, strong convection, drizzle, and extratropical transition. During the measurement periods, disdrometric data from all rain situations are selected rather than choosing specific events.

b. Radar data

The McGill S-band scanning radar has been upgraded to dual-polarization in 1999 and has been measuring polarimetric parameters in real time. It transmits a 45° linearly polarized beam and receives horizontal (H) and vertical (V) components simultaneously with two receivers; that is, it uses the simultaneous sampling method. According to Gingras et al. (1997), this method provides relatively smaller measurement errors in polarimetric parameters compared with the nonsimultaneous sampling method (i.e., switched H/V on transmit and copolar receive). Because the McGill S-band radar is a part of the Canadian operational radar network, it scans at the speed of 6 rotations per minute (rpm) or 36° s⁻¹ to maximize the volumetric surveillance. After a few months of upgrade, the horizontal channel lost its sensitivity because of damage in the rotary joint. The rotary joint was replaced in September 2001 and since then there is only a few decibels difference in the horizontal and vertical channels. The radar calibration has been regularly checked with the GEs, gauges, nearby POSS, and polarimetry. A detailed methodology on disdrometric and polarimetric calibration methods is described in Lee and Zawadzki (2005c). Five events of heavy rain have been selected after the replacement of the rotary joint. The five events are (i) 0550–0950 UTC 13 September 2001, (ii) 2030 UTC 24 September–0430 UTC 25 September 2001, (iii) 2100 UTC 8 July–0200 UTC 9 July 2002, (iv) 0452–1052 UTC September 2002, and (v) 0230–0530 UTC 23 September 2002. They include strong convective cells or lines and are accompanied by stratiform rain. As mentioned, all polarimetric parameters are collected at 6 rpm with a spatial resolution of 1° × 150 m and are

degraded to $1^\circ \times 1$ km for archive purpose. The data quality is carefully controlled to avoid possible contamination by ground echo using the polarimetric target identification of Zawadzki et al. (2001), Doppler radial velocity, and the normal ground echo mask. To avoid a possible contamination by the bright band (BB), data are excluded when the 3-dB edge of the radar beam intercepts the brightband limits. All data are composed of 312 plan position indicators (PPIs) at 0.9° for 26 h. The distance between the POSS and scanning radar was about 30 km.

3. Errors in rain estimation from polarimetric parameters

In this section, we investigate errors in rain estimation resulting from the variability of DSDs alone. Similar investigations have assumed a specific DSD model and the usual range of model parameters (Sachidananda and Zrnica 1987; Bringi et al. 1990; Chandrasekar et al. 1990; Ryzhkov and Zrnica 1995; Zrnica et al. 2000; Gorgucci et al. 2002). Only a few studies are performed with measured DSDs (Seliga et al. 1986; Balakrishnan et al. 1989; Keenan et al. 2001). However, their dataset is limited (only a few storms) and is affected by the undersampling effect of disdrometers so that it hardly represents overall DSD variability, even in a single climatic regime.

Instead of assuming a specific DSD (exponential or gamma) model, we use actual measurements of DSDs to fully maintain the physical variability of DSDs. From a 5-yr disdrometric dataset (20 400 one-minute DSDs) measured by POSS in Montreal, polarimetric parameters (Z_h , Z_{DR} , K_{DP}) for S band (10.4 cm; equivalent to the wavelength of the McGill S-band operational scanning radar) are calculated with a scattering model (Mishchenko et al. 2000) by assuming the drop deformation formula of Pruppacher and Beard (1970) and a temperature of 10°C . This scattering model has been widely tested and the results are consistent with those from another scattering model used by Torlaschi and Zawadzki (2003). The rainfall intensity R is derived from DSDs using the following equation:

$$R = 6\pi \times 10^{-4} \int_{D_{\min}}^{D_{\max}} v(D) D^3 N(D) dD, \quad (1)$$

where D (mm) is the diameter of drops, $N(D)$ ($\text{m}^{-3} \text{mm}^{-1}$) is the number of drops per unit volume and diameter interval dD (mm), and $v(D)$ (m s^{-1}) is the terminal fall velocity according to Gunn and Kinzer (1949). Relationships between R and polarimetric parameters are subsequently derived by a least squares

regression. Using these relationships, the “transformed” rainfall intensity R_T is obtained from polarimetric parameters and is compared with R from (1). The scatterplot of R and R_T is shown in Fig. 1 for selected relationships. All derived relationships and statistics are shown in Table 1. The standard deviation (SD) and the standard deviation of fractional error (SDFE) are given by

$$\begin{aligned} \text{SD} &= \left\{ \frac{1}{k} \sum (R - R_T)^2 \right\}^{1/2} \quad \text{and} \\ \text{SDFE} &= \left\{ \frac{1}{k} \sum \left(\frac{R - R_T}{R} \right)^2 \right\}^{1/2}, \end{aligned} \quad (2)$$

where k is the number of comparisons. The standard deviation has large weight in heavy rain while SDFE has the same weight for all ranges of rain intensity. Hence, the former is a better representation of the accuracy in moderate to heavy rain while SDFE better reflects the accuracy in light to moderate rain. The same error analysis is performed for half of the dataset selected randomly. Results are consistent with those from the whole dataset. This indicates that our sample size is sufficiently large to yield robust results.

In the one-parameter approach with Z_h (Fig. 1a), an appreciable amount of scatter is present ($\text{SD} = 3.7 \text{ mm h}^{-1}$ and $\text{SDFE} = 61\%$) because of the variability of DSDs. Using the polarimetric parameter K_{DP} (Fig. 1b), the scatter significantly decreases ($\text{SD} = 2.3 \text{ mm h}^{-1}$ and $\text{SDFE} = 34\%$). In fact, K_{DP} can be approximated with the 4.6th moment ($M_{4.6}$) of DSDs for the drop shape of Pruppacher and Beard (1970). Assuming $v(D) = 3.778D^{0.67}$, $R \sim M_{3.67}$. Hence, the effect of the DSD variability is less pronounced in rain estimation with the R - K_{DP} relationship than that with the R - Z_h relationship. However, a significant amount of scatter is still maintained because the DSD variability is still appreciable.

The DSD variability cannot be fully explained by one parameter, and a second parameter is needed (Sekhon and Srivastava 1971; Waldvogel 1974; Seliga and Bringi 1976; Willis 1984; Testud et al. 2001; Lee et al. 2004). This points to the advantage of dual-parameter rain estimation. For our entire DSD database, results from various combinations of polarimetric parameters are shown in Figs. 1c-f with a summary of statistics and relationships in Table 1. In general, the scatter is significantly decreased ($\text{SD} \leq 1.8 \text{ mm h}^{-1}$ and $\text{SDFE} \leq 23\%$), except for the relationship $R = aZ_h^b Z_{DR}^c$ (not shown in Fig. 1 and relationship 3 in Table 1). Furthermore, various relationships show interesting characteristics. The scatterplots for the two relationships with Z_h and Z_{DR} (Figs. 1c and 1d) show that a form of 10

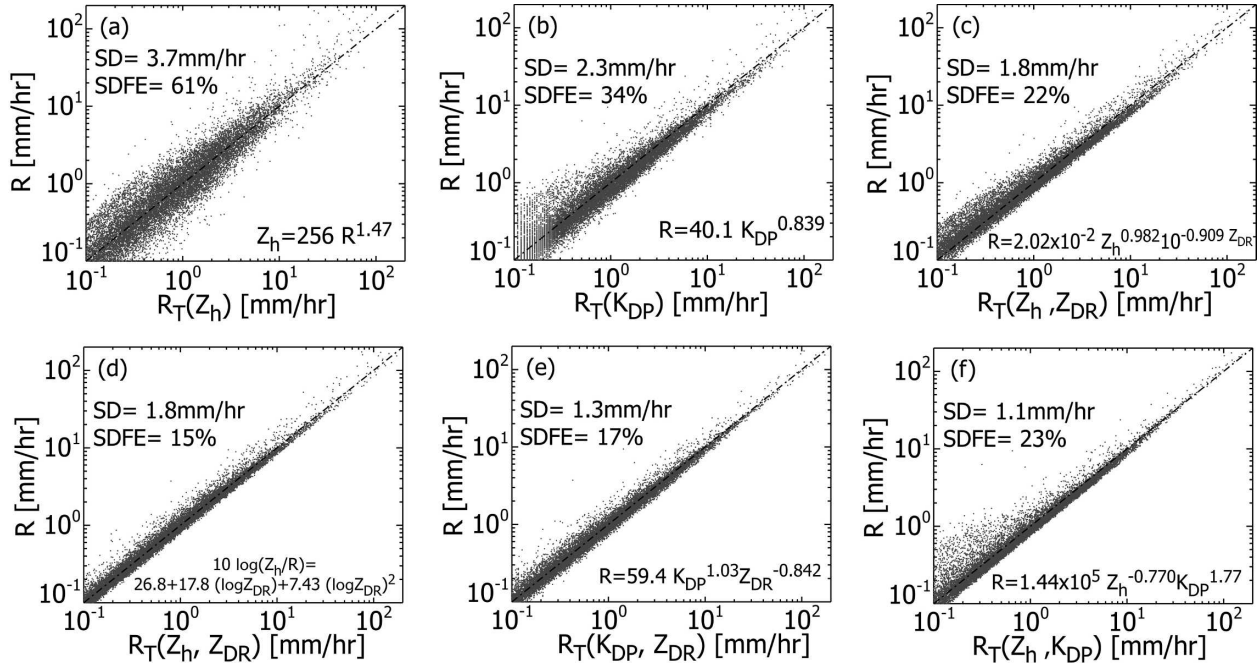


FIG. 1. Scatterplot of R derived from 1-min DSDs and R_T estimated from various combinations of polarimetric parameters. The relationships used to estimate R are first derived from the 5-yr disdrometric dataset. Using these derived relationships, R_T is then obtained from the same dataset. The scatter illustrates the effect of the DSD variability in the estimation of rainfall rate.

$\log(Z_h/R) = f(\log Z_{DR})$ estimates R more accurately than the conventional form of the formula ($R = aZ_h^b Z_{DR}^c$ or $R = dZ_h^e 10^{fZ_{DR}}$) at $R < 20 \text{ mm h}^{-1}$ (SD = 1.8 mm h⁻¹ and SDFE = 15%). [Because from the data $10 \log(Z_h/R)$ is better correlated to $\log Z_{DR}$ than Z_{DR} , we choose

this form instead of $10 \log(Z_h/R) = f(Z_{DR})$, as suggested by Illingworth and Blackman (2002).] However, as indicated by the relatively large standard deviation, a significant scatter is still present at $R > 20 \text{ mm h}^{-1}$. With a combination of (K_{DP}, Z_{DR}) or (Z_h, K_{DP}) in

TABLE 1. Errors and derived relationships in the estimation of the rainfall rate with one or two polarimetric parameters. The same dataset as in Fig. 1 is used and DSDs with reflectivity smaller than 10 dBZ are excluded. SD and SDFE are defined in (2). SIFT represents the “sequential intensity filtering technique” with $M = 10$ one-minute DSDs and $W = 1 \text{ h}$. The error represents the theoretical limit of rain estimation with a single- or double-parameter technique resulting from the variability of DSDs.

	Relationships	SD (mm h ⁻¹)	SDFE (%)
1-min DSDs	1: $R = 2.33 \times 10^{-2} Z_h^{0.678}$ ($Z_h = 256 R^{1.47}$), Fig. 1a	3.7	61
	2: $R = 40.1 K_{DP}^{0.839}$, Fig. 1b	2.3	34
	3: $R = 3.32 \times 10^{-3} Z_h^{0.940} Z_{DR}^{-1.13}$, not shown	2.6	27
	4: $R = 2.02 \times 10^{-2} Z_h^{0.982} 10^{-0.909 Z_{DR}}$, Fig. 1c	1.8	22
	5: $10 \log(Z_h/R) = 26.8 + 17.8 \log Z_{DR} + 7.43 (\log Z_{DR})^2$, Fig. 1d	1.8	15
	6: $R = 59.4 K_{DP}^{1.03} Z_{DR}^{-0.842}$, Fig. 1e	1.3	17
	7: $R = 132 K_{DP}^{0.958} 10^{-0.441 Z_{DR}}$, not shown	1.3	21
	8: $R = 1.44 \times 10^5 Z_h^{-0.770} K_{DP}^{1.77}$, Fig. 1f	1.1	23
SIFT DSDs	9: $R = 2.34 \times 10^{-2} Z_h^{0.683}$ ($Z_h = 244 R^{1.46}$)	2.2	38
	10: $R = 40.8 K_{DP}^{0.850}$	1.4	25
	11: $R = 3.62 \times 10^{-3} Z_h^{0.936} Z_{DR}^{-1.15}$	1.6	17
	12: $R = 2.00 \times 10^{-2} Z_h^{1.01} 10^{-0.988 Z_{DR}}$	1.1	18
	13: $10 \log(Z_h/R) = 26.5 + 17.9 \log Z_{DR} + 7.69 (\log Z_{DR})^2$	1.3	13
	14: $R = 61.6 K_{DP}^{1.04} Z_{DR}^{-0.875}$	0.81	14
	15: $R = 185 K_{DP}^{1.01} 10^{-0.520 Z_{DR}}$	0.79	18
	16: $R = 3.76 \times 10^5 Z_h^{-0.861} K_{DP}^{1.87}$	0.57	19

Figs. 1e and 1f, the scatter at $R > 10 \text{ mm h}^{-1}$ is significantly reduced, although the scatter at R of less than a few millimeters per hour increases compared with the form of the $10 \log(Z_h/R) = f(\log Z_{\text{DR}})$ relationships. This reduction is indicated by the small standard deviation ($\text{SD} \leq 1.3 \text{ mm h}^{-1}$). These results suggest a hybrid algorithm for rainfall estimation, that is, the form of the $10 \log(Z_h/R) = f(\log Z_{\text{DR}})$ relationship for $R < 5 \text{ mm h}^{-1}$ and $R = aK_{\text{DP}}^b Z_{\text{DR}}^c$ (Fig. 1e) or $R = eZ_h^f K_{\text{DP}}^k$ (Fig. 1f) for $R > 5 \text{ mm h}^{-1}$. Because K_{DP} is quite small (less than $0.1^\circ \text{ km}^{-1}$) and noisy when $R < 5 \text{ mm h}^{-1}$, the use of Z_{DR} in addition to Z_h is quite advantageous with light rain in terms of reducing the DSD variability. However, as shown in section 5, a detailed analysis on the propagation of measurement errors is necessary before concluding on the success of the form of the $10 \log(Z_h/R) = f(\log Z_{\text{DR}})$ relationship for light rain. In addition, R estimation with $R = eZ_h^f K_{\text{DP}}^k$ is quite sensitive to the assumed formula of drop deformation. Hence, the relationship $R = aK_{\text{DP}}^b Z_{\text{DR}}^c$ is preferable for $R > 5 \text{ mm h}^{-1}$, as suggested by Ryzhkov and Zrnic (1995).

The disdrometric measurements are affected by “observational and instrumental noise” resulting from drop sorting and small sampling volume (Chandrasekar and Bringi 1987; Smith et al. 1993; Joss and Zawadzki 1997; Lee and Zawadzki 2005a). Hence, the above analysis is affected by disdrometric measurement errors. The sampling volume of POSS is three orders of magnitude larger than that of other disdrometers so that the instrumental noise resulting from statistical undersampling is a second-order problem. The observational noise resulting from the drop sorting depends on the spatial structure of precipitation and dynamical fields. However, this noise is less significant in measurement from scanning radars that have a large sampling volume ($\sim 1 \text{ km}^3$) and sample rain fields instantaneously. To eliminate the spurious variability while keeping the physical variability in DSD measurements, Lee and Zawadzki (2005a) applied a sequential intensity filtering technique (SIFT). SIFT is a moving average of M 1-min DSDs, within a window of a specified time interval W , and is ordered by increasing reflectivity. SIFT can be applied simultaneously in space and time. For polarimetric measurements, the noise in polarimetric parameters can be filtered out by averaging within a narrow interval of reflectivity. For example, an average of Z_{DR} is obtained from data points of similar reflectivity data points within a window ($W = 10^\circ \times 10 \text{ km} \times 10 \text{ min}$). Then, the averaged Z_{DR} is transformed into R . Thus, the measurement noise is reduced prior to the transformation. SIFT is a way of analyzing noisy data. However, it reduces the physical variability by smooth-

ing the physical variation of Z_{DR} within the interval of reflectivity. This reduction could be more pronounced with a large window in which different physical processes coexist. Thus, the use of proper windows and averaging sizes is essential in order to minimize the filtering of the physical variability. Because the multiparameter relationships from SIFT are independent of the averaging size (appendix B), any flexible number of data points can be averaged.

We derive the stable multiparameter relationships that are independent of the averaging time. Specifically, SIFT is applied for each day as a moving average of 10 one-minute DSDs ($M = 10$) after they have been ordered in terms of increasing Z within a time window of 1 h ($W = 1 \text{ h}$). The same analysis as in Fig. 1 is performed with these filtered DSDs. The statistics and derived relationships are shown in Table 1 and are indicated by “SIFT DSDs.” After applying SIFT, the physical variability is smoothed out and the time scale becomes uncertain. However, an error analysis shows that the DSD variability of SIFT DSDs is similar to that of 30-min-averaged DSDs (see Figs. 2b and 4 of Lee and Zawadzki 2005b). Thus, the derived statistics should be interpreted at a similar time scale.

With a single parameter, SD and SDFE are drastically reduced after applying SIFT as a consequence of noise elimination and filtering of some physical variability. The reduction of SDFE is especially pronounced with the $R - Z_h$ relationship. However, SD shows that about 60% of the original variance is reduced by SIFT. In other words, there is no preferential decrease of SD in the $R - Z_h$ relationship. The relationship $R = dZ_h^e K_{\text{DP}}^f$ (relationship 16, Table 1) provides the smallest standard deviation, indicating the best estimation of R for heavy rain. As indicated by $\text{SDFE} = 13\%$ and $\text{SD} = 1.3 \text{ mm h}^{-1}$, the form of $10 \log(Z_h/R) = f(\log Z_{\text{DR}})$ (relationship 13, Table 1) accurately estimates R for light rain and this accuracy degrades with increasing R . With K_{DP} and Z_{DR} (relationship 14, Table 1), SD and SDFE are both relatively small. In fact, after applying SIFT, any two polarimetric parameters yield $\text{SD} < 1.6 \text{ mm h}^{-1}$ and $\text{SDFE} < 20\%$, regardless of the relationships used. Thus, these results suggest that additional polarimetric parameters can significantly improve the accuracy in R even after applying SIFT for noisy data. From a practical point of view, we need to determine which of the available parameters are most free of measurement errors.

4. Comparison of the derived relationships with those from literature

The relationships between R and polarimetric parameters are derived here from a large dataset that

TABLE 2. Relationships suggested in the literature and some characteristics.

Literature	Relationship	Drop deformation formula	DSD model
Chandrasekar and Bringi (1988)	$R = 0.002397Z_h^{0.94}Z_{DR}^{-1.08}$	Pruppacher and Beard (1970)	Gamma
Chandrasekar et al. (1990)	$R = 0.00198Z_h^{0.97}Z_{DR}^{-1.05}$	Green (1975)	Gamma
Bringi et al. (2003)	$R = 0.00347Z_h^{0.945}Z_{DR}^{-1.457}$	Green (1975)	Gamma
Jameson (1994)	$Z_h/R = -14\,597.133\zeta^6 + 103\,891.25\zeta^5$ $- 281\,075.94\zeta^4 + 344\,285.59\zeta^3 - 147$ $125.05\zeta^2 - 48\,763.69\zeta + 43\,599.19$ where $\zeta = Z_h/Z_v$	Pruppacher and Beard (1970)	Gamma
Ryzhkov and Zrnica (1995)	$R = 57.4K_{DP}^{0.935}Z_{DR}^{-0.704}$ (all range of R) (RZ1) $R = 52.0K_{DP}^{0.960}Z_{DR}^{-0.447}$ ($R > 20 \text{ mm h}^{-1}$) (RZ2)	Pruppacher and Beard (1970)	Gamma
Ryzhkov et al. (2005)	$R = 0.0159Z_h^{0.737}\zeta^{-1.03}$	Andsager et al. (1999)	Measured DSDs
Ryzhkov et al. (2005)	$R = 63.3 K_{DP} ^{0.851}\zeta^{-0.72}\text{sign}(K_{DP})$	Andsager et al. (1999)	Measured DSDs
Illingworth and Blackman (2002)	$Z_h/R = 21.48 + 8.14Z_{DR} - 1.385Z_{DR}^2$ $+ 0.1039Z_{DR}^3$	Goddard et al. (1995)	Normalized gamma

includes a variety of rain situations. However, most relationships in the literature are derived from a model DSD (the exponential or gamma function) with assumed ranges of parameters of this DSD model (Sachidananda and Zrnica 1987; Chandrasekar and Bringi 1988; Chandrasekar et al. 1990; Jameson 1994; Ryzhkov and Zrnica 1995). Recently these relationships have been obtained from a large dataset of measured DSDs in a single climate (Ryzhkov et al. 2005). The range of parameters in the gamma DSD model [i.e., N_0 , λ , and μ of $N(D) = N_0 D^\mu e^{-\lambda D}$] was first derived by Ulbrich (1983) from the exponents and coefficients of R - Z relationships shown in Battan (1973). However, the R - Z relationships are subject to a large uncertainty (40% of natural variability reported in the literature) because of the use of nonadequate regression methods in the presence of the scatter in R - Z plots (Lee and Zawadzki 2005a). Hence, the derived range of the DSD parameters may be doubtful. Illingworth and Blackman (2002) illustrate that this range is unrealistic and the relationship $R = aZ_h^b Z_{DR}^c$ in the literature derived from this unrealistic range yields an error of 3 dB in the estimation of R . Furthermore, they argue that by using the normalized form of gamma DSDs and a new range of parameters of normalized DSDs, a new derived relationship provides an error of 25% in R . Later, Bringi et al. (2003) argued that some results of Illingworth and Blackman (2002) were because of the overreliance on the drop shape of Goddard et al. (1995). They also showed that the Ulbrich (1983) range of the gamma parameters is realistic. The use of a specific DSD model may be useful in term of mathematical manipulation or of microphysical parameterization in numerical models, but this procedure smoothes out the physical variability of DSDs. For example, the gamma DSD cannot describe the S-shaped DSD frequently observed in con-

vective situations (Fig. 7 of Sauvageot and Lacaux 1995; Fig. 10 of Uijlenhoet et al. 2003; Fig. 4.7 of Lee 2003; Fig. 1 of Montero-Martinez and Garcia-Garcia 2004; Fig. 6 of Zawadzki and Lee 2004) and the bimodal DSDs, and hence the gamma fit to these DSDs eliminates the physical DSD variability. As a result, model error is added to the other sources of uncertainty.

We now compare our derived relationships with those from the literature that are derived from the DSD models and measured DSDs in different climatic regimes. This comparison should inform us of the applicability of these relationships in the Montreal region and of the stability of the multiparameter relationships in these different regimes and different methods of derivation. Table 2 summarizes the relationships shown in the literature. Six formulas use Z_h and Z_{DR} , while the other three use K_{DP} and Z_{DR} . Chandrasekar et al. (1990) used the drop deformation by Green (1975), which is similar to that of Pruppacher and Beard (1970). The relationship from Chandrasekar and Bringi (1988) is similar to that of Chandrasekar et al. (1990) and hence is not included in the comparison. Note that, although different from Chandrasekar et al. (1990), the relationship from Bringi et al. (2003) is optimized for the rain estimation (Chandrasekar et al. 1993; Gorgucci et al. 1995). Illingworth and Blackman (2002) used the formula of Goddard et al. (1995) for drop shape. Ryzhkov et al. (2005) used the drop shape of Andsager et al. (1999) at $1.1 \text{ mm} < D < 4.4$ and the multiyear statistics of measured DSDs at central Oklahoma. Figure 2 shows a comparison of these relationships for the same category of drop deformation [Figs. 2a,b: Pruppacher and Beard (1970); Fig. 2c: Goddard et al. (1995)] and for the same combination of polarimetric parameters (Fig. 2a,c: Z_h and Z_{DR} ; Fig. 2b: K_{DP} and Z_{DR}) used. The relationships from Ryzhkov et al. (2005) are not shown

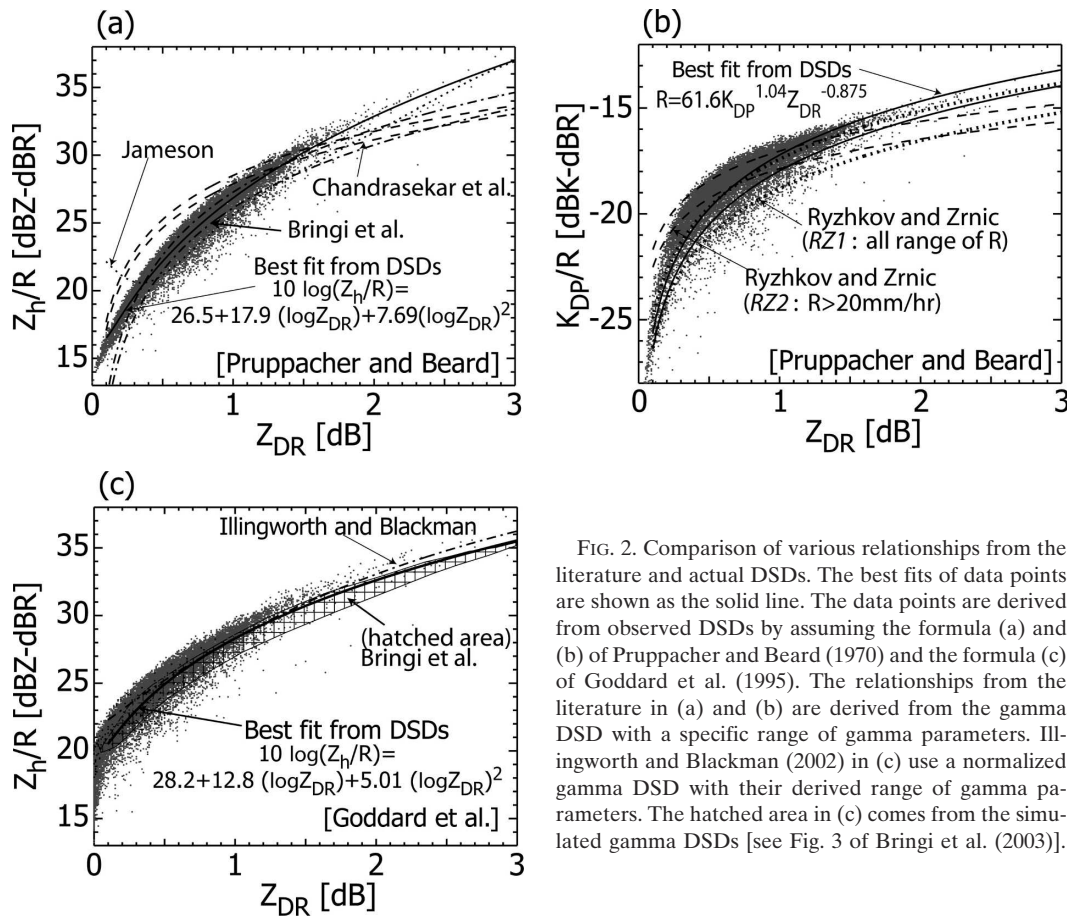


FIG. 2. Comparison of various relationships from the literature and actual DSDs. The best fits of data points are shown as the solid line. The data points are derived from observed DSDs by assuming the formula (a) and (b) of Pruppacher and Beard (1970) and the formula (c) of Goddard et al. (1995). The relationships from the literature in (a) and (b) are derived from the gamma DSD with a specific range of gamma parameters. Illingworth and Blackman (2002) in (c) use a normalized gamma DSD with their derived range of gamma parameters. The hatched area in (c) comes from the simulated gamma DSDs [see Fig. 3 of Bringi et al. (2003)].

in the figure and are used to derive statistics. The scatter of points is derived from the disdrometric data using the indicated formulas of drop deformation [Figs. 2a and 2b: Pruppacher and Beard (1970); Fig. 2c: Goddard et al. (1995)]. The solid lines indicate the best fit of these points. When the exponent of Z_h or K_{DP} is not equal to 1, the equation cannot be expressed as a single line in the diagram. For this case, we draw two lines of the same style corresponding to two rainfall intensities, $R = 1 \text{ mm h}^{-1}$ (pointed by an arrow) and 100 mm h^{-1} . For example, for the relationship of Chandrasekar et al. (1990) in Fig. 2a, the lower dashed line (pointed by an arrow) is derived with $R = 1 \text{ mm h}^{-1}$ and the upper dashed with $R = 100 \text{ mm h}^{-1}$. The hatched area in Fig. 2c comes from the simulated DSDs with the gamma model (see Fig. 3 of Bringi et al. 2003).

The deviation from the best-fit curve to the data is quite pronounced for most relationships except for those from Bringi et al. (2003) and Illingworth and Blackman (2002). The deviation from the best-fit curve indicates bias, that is, an underestimation when the lines are above the best fit and vice versa. In Fig. 2a, an underestimation of R for a given Z_h and Z_{DR} is ex-

pected when $Z_{DR} < 1.5 \text{ dB}$ with the relationship of Chandrasekar et al. (1990). For example, the underestimation is around 1.5–2 dB (~40%–60%) at $Z_{DR} = 1 \text{ dB}$. However, a small bias (<1 dB) is expected at $0.5 \text{ dB} < Z_{DR} < 1 \text{ dB}$ with the relationship of Bringi et al. (2003). In general, this relationship slightly overestimates R . When compared with results from the relationship of Chandrasekar et al. (1990), the optimization of the relationship for R estimate (Chandrasekar et al. 1993; Gorgucci et al. 1995) significantly reduces the bias. However, as shown by the hatched area in Fig. 2c, the simulated DSDs represent only a portion of the overall data area. Thus, the simulated DSDs cannot provide the full natural variability observed in Montreal. An overestimation of around 1 dB is introduced by using the relationship from Jameson (1994) at $0.5 \text{ dB} < Z_{DR} < 2.5 \text{ dB}$. For the form of $R = aK_{DP}^b Z_{DR}^c$ (Fig. 2b), the two relationships (RZ1 and RZ2) from Ryzhkov and Zrnice (1995) show different trends. As indicated by the dotted line (pointed by the arrow), a significant overestimation is noticed for RZ1 derived from all ranges of R . However, RZ2 derived when $R > 20 \text{ mm h}^{-1}$ is close to the best fit when $0.5 \text{ dB} < Z_{DR} < 1.5 \text{ dB}$.

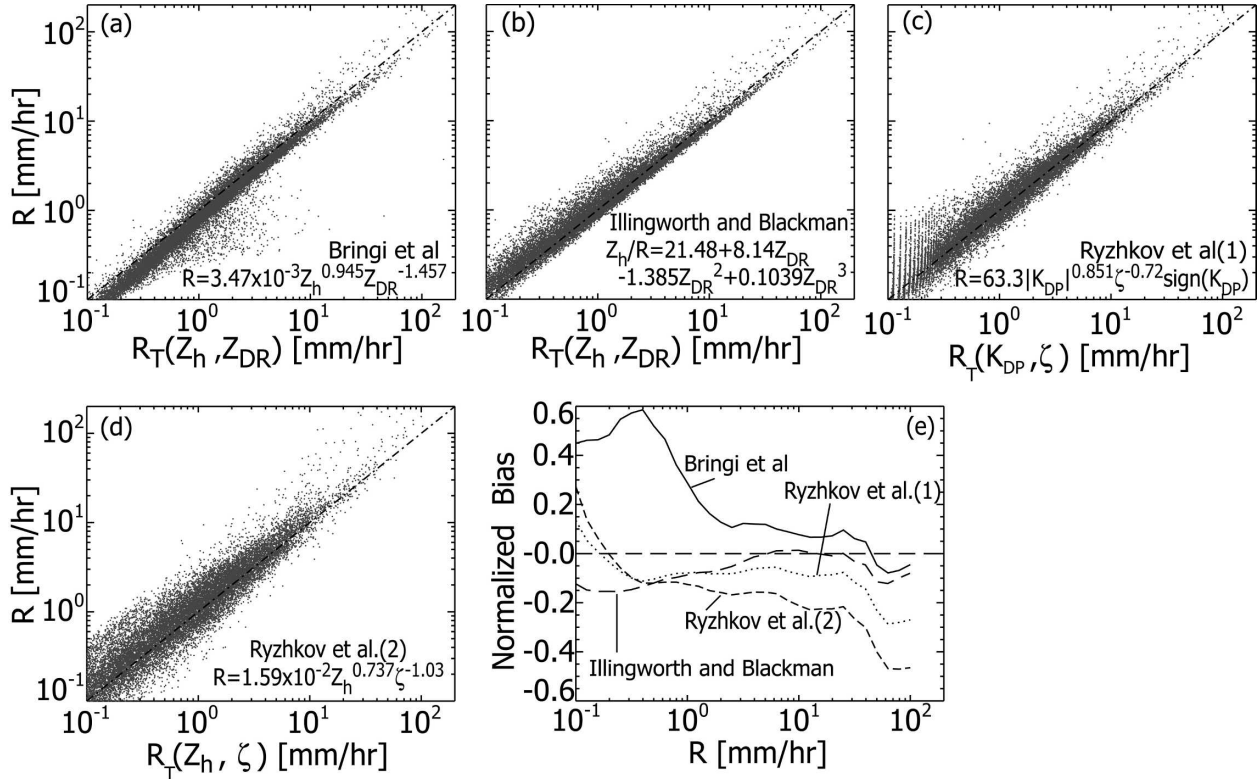


FIG. 3. (a)–(d) Scatterplot of R derived from observed DSDs and R_T estimated from the various relationships suggested in the literature, and the (e) normalized bias calculated from (a)–(d).

The relationship of Illingworth and Blackman (2002) (dotted line in Fig. 2c), derived from the normalized gamma DSDs with a new range of parameters of DSDs, is quite close to the best fit over the wide interval $0.5 \text{ dB} < Z_{\text{DR}} < 2 \text{ dB}$, indicating no significant bias. The relationships from Ryzhkov et al. (2005) are significantly different from $R = 246 K_{\text{DP}}^{1.01} 10^{-0.523 Z_{\text{DR}}}$ and $R = 0.0101 Z_{\text{h}}^{0.993} 10^{-0.846 Z_{\text{DR}}}$, which are derived from our data with the drop shape of Goddard et al. (1995).

Using the disdrometric dataset, we now quantify the bias resulting from the deviation of these relationships from the best fit. The scatterplot of R , derived from the observed DSDs, with R_T as estimated from the various relationships listed in Table 2, is shown in Fig. 3. Note that an underestimation is indicated by data points above the diagonal line and vice versa. The normalized bias is defined as follows from the scatterplot:

$$\text{Normalized bias} = \frac{\frac{1}{k} \sum (R_T - R)}{\frac{1}{k} \sum R}. \quad (3)$$

Results from four relationships are only shown. By using the relationship from Bringi et al. (2003), as shown

in Fig. 3a, an overestimation of about 10% is introduced when $2 \text{ mm h}^{-1} < R < 30 \text{ mm h}^{-1}$ and a large overestimation ($>20\%$) is shown for moderate rain ($<1 \text{ mm h}^{-1}$). When compared with Fig. 1c, the scatter (random error) slightly increases. A significant bias is obtained with the relationships by Jameson (1994), Chandrasekar et al. (1990), and RZ1. As expected from Fig. 2c, the relationship from Illingworth and Blackman (2002) does not introduce any significant bias (less than 10%) for a wide range of R , $1 \text{ mm h}^{-1} < R < 40 \text{ mm h}^{-1}$. The bias slightly increases when $R < 0.5 \text{ mm h}^{-1}$ and $R > 50 \text{ mm h}^{-1}$, as indicated by a deviation of the relationship from the best fit (Fig. 2c). However, the random error significantly increases (see Figs. 1d and 3b). The relationships from Ryzhkov et al. (2005) show a bias of $\sim 10\%$ – 20% for a wide range of R . In addition, the increase of the random error is noticeable, particularly for the $R = a Z_{\text{h}}^b \zeta^c$ relationship. The degree of scatter in Fig. 3d is comparable with $R - Z_{\text{h}}$ relationship in Fig. 1a.

In summary, except for the relationship derived from the normalized gamma DSD and the optimized relationship, all other DSD models yield a significant bias. [It was not clear in the literature whether the optimi-

zation procedure was applied for the other relationships from Jameson (1994) and Ryzhkov and Zrnic (1995).] The relationships of measured DSDs in central Oklahoma show a bias of $\sim 10\%$ – 20% . In addition, the random error significantly increases. These results suggest an important issue on *the variation of multiparameter relationships in different climate regimes*. Bringi et al. (2003) stated “the Ulbrich range of DSDs is better suited for tropical rain than for midlatitude continental rain.” (The author thinks that the range should be more relevant for the global average because it was derived from various R – Z in different climate regimes.) We have compared relationships from four different climate regimes [Tropics for Bringi et al. (2003), the United Kingdom for Illingworth and Blackman (2002), Oklahoma for Ryzhkov et al. (2005), and Montreal for our analysis]. Thus, the systematic change of the multiparameter relationships in different climate regimes provides a systematic bias of $\sim 10\%$ – 20% and significant random errors. Because the stratiform precipitation is dominant in the United Kingdom and Montreal, similar relationships are more reasonable. In Oklahoma, where strong convective precipitation is dominant, the relationship could be significantly different from that of Montreal.

5. Relative importance of the DSD variability and measurement noise

The variability of the measured polarimetric parameters by scanning radar is a combined effect of the DSD variability and of the measurement noise. When the latter is a significant fraction of the variation of K_{DP} and Z_{DR} resulting from the DSD variability, the application of these measurements causes an additional uncertainty in rain estimation. Furthermore, the reduction of the DSD variability using these parameters could be masked by measurement noise. Sachidananda and Zrnic (1987) tried to evaluate the degree of observational noise by comparing the scatterplot of Z_h and Z_{DR} or K_{DP} from actual measurements and the DSD variability. They used simulated DSDs to derive the DSD variability. As they alluded, and as shown in Fig. 2c, the DSD variability is quite limited by using simulated DSDs from the gamma model, and their simulated DSDs do not fully describe the natural variability of DSDs in Montreal. In this section, we quantify the effect of DSD variability on polarimetric parameters from actual disdrometric measurements rather than from a specific DSD model. This effect is compared with the measurement noise deduced from the literature as well as from actual measurements by the McGill S-band operational polarimetric radar.

a. Variation of Z_{DR} resulting from the DSD variability

Figure 4 shows a scatterplot of Z_{DR} and Z_h from 5 yr of disdrometric data and the SD and the normalized standard deviation (NSD) as a function of average Z_h at 2-dBZ intervals. Both SD and NSD are obtained with respect to the average differential reflectivity $Z_{DR,avg}$ (solid line). The detailed frequency distributions of $(Z_{DR,avg} - Z_{DR})$ and its comparison with a Gaussian distribution are shown in appendix C. The $Z_{DR} - Z_h$ pairs (circles in Figs. 4a and 4c) are derived from the average DSDs of the entire dataset in 2-dB intervals of Z_h . Results from M – P DSDs (dashed line) and \pm SD (vertical bars) are also shown. The Z_{DR} from M – P DSDs is higher than the one from average DSDs, particularly when $Z_h > 35$ dBZ, indicating that the M – P DSDs have a greater concentration of larger drops than the average DSDs. The scatter representing the effect of the DSD variability on Z_{DR} is quite small. Here SD ~ 0.2 dB for $Z_h < 37$ dBZ, then peaks at 0.3 dB around $Z_h = 43$ dBZ. NSD decreases with Z_h , remaining of the order of 20% for $Z_h > 30$ dBZ.

The scatter in Fig. 4a is the final outcome of the disdrometric measurement noise and physical variability of DSDs. From appendix A, the instrumental noise of the differential reflectivity resulting from the undersampling effect and retrieval algorithm should be less than 0.068 dB for 1-min DSDs. Thus, about 88%–95% of the variance could be due to the physical variability of DSDs when we neglect the measurement noise caused by wind effects. As the temporal averaging interval increases, the contribution from the DSD measurement noise should become negligible (appendix A) and the remaining scatter should be the result of only the physical variability. A similar analysis for 30-min-averaged DSDs shows the reduction of the scatter. This reduction is related to the elimination of DSD measurement noise and the filtering of some physical variability. Because the DSD measurement noise is insignificant at this temporal smoothing, the overall scatter should be due to the physical variability. The results show SD ~ 0.19 dB for $Z_h < 22$ dBZ, decreasing to 0.15 dB for 25 dBZ $< Z_h < 30$ dBZ, and then peaking at 0.22 dB around $Z_h = 41$ dBZ. NSD is less than 18% for $Z_h > 30$ dBZ. In practice, the accuracy in Z_{DR} calibration is around 0.1–0.2 dB, achieved with a polarimetric radar pointing vertically to which a random measurement noise must be added. Thus, this accuracy is quite comparable with the SD because of the physical variability with an averaging time of 30 min. When the degree of measurement noise is similar to the SD because of the DSD variability, we cannot expect a sig-

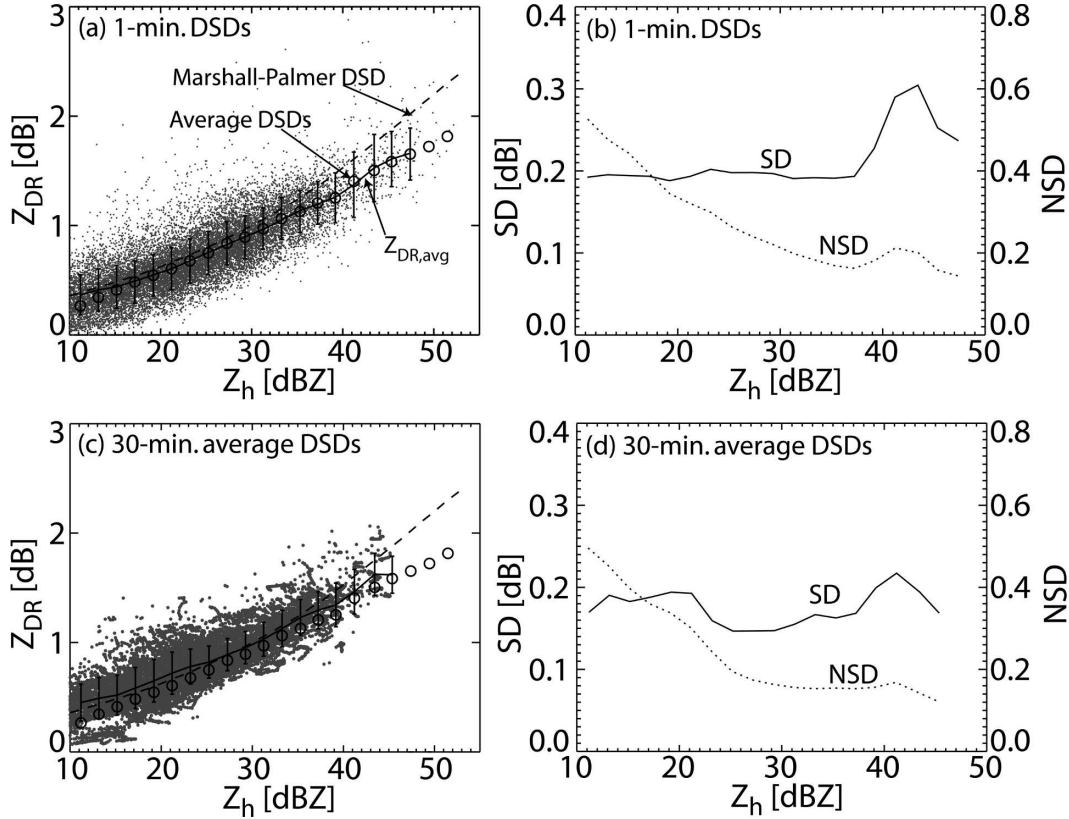


FIG. 4. (a), (c) Scatterplot of Z_{DR} and Z_h calculated from 1- and 30-min-averaged disdrometric data. Here $Z_{DR,avg}$ indicates the average Z_{DR} for 2-dB intervals of Z_h . The dashed line is derived from Marshall and Palmer (1948) DSDs and the circles from average DSDs of 5-yr data at 2-dBZ intervals. The vertical bars indicate the standard deviation of Z_{DR} . (b), (d) SD and NSD in estimating Z_{DR} with respect to $Z_{DR,avg} - Z_h$ pairs.

nificant improvement in rain estimation, and the reduction of the DSD variability by using polarimetric information is masked by the measurement noise. Thus, the measurement noise should be kept less than the SD in Z_{DR} shown in Fig. 4.

b. Errors in R resulting from the DSD variability and measurement noise

The accuracy in estimating R is affected by the DSD variability as well as measurement noise in polarimetric parameters. Similar to the DSD variability, the measurement noise in polarimetric parameters propagates into the estimation of R . When y is a function of two variables $y = f(x_1, x_2)$, the uncertainty in y can be expressed in terms of the uncertainty in x_1 and x_2 (Bevington 1969),

$$\sigma_y^2 \cong \sigma_{x_1}^2 \left(\frac{\partial y}{\partial x_1} \right)^2 + \sigma_{x_2}^2 \left(\frac{\partial y}{\partial x_2} \right)^2 + 2\sigma_{x_1 x_2}^2 \left(\frac{\partial y}{\partial x_1} \right) \left(\frac{\partial y}{\partial x_2} \right), \quad (4)$$

where σ_y is the standard deviation of y resulting from the measurement errors σ_{x_1} and σ_{x_2} ; $\sigma_{x_1 x_2}^2$ is the covariance between x_1 and x_2 . When R is estimated from two polarimetric parameters as in $R = aK_{DP}^b Z_{DR}^c$, we can express the normalized standard deviation σ_R/R with the following equation:

$$\frac{\sigma_R}{R} = \left\{ \left(b \frac{\sigma_{K_{DP}}}{K_{DP}} \right)^2 + \left(c \frac{\sigma_{Z_{DR}}}{Z_{DR}} \right)^2 \right\}^{1/2}. \quad (5)$$

Here, we assume that the measurement noise in K_{DP} and Z_{DR} is uncorrelated ($\sigma_{x_1 x_2}^2 = 0$). This equation illustrates the propagation of the measurement error in K_{DP} and Z_{DR} into the estimation of R . Using this equation and an assumed measurement noise of $\sigma_{Z_h} = 1.0$ dB, $\sigma_{Z_{DR}} = 0.17$ dB, and $\sigma_{K_{DP}} = 0.11^\circ \text{ km}^{-1}$, the uncertainty ($\sigma_{R,obs}/R$) resulting from this noise is calculated for the four relationships shown in Table 1 (relationships 9, 10, 13, 14). The results are shown as dashed lines in Fig. 5.

According to Gorgucci et al. (2002), given an accuracy of 2.5° in differential phase shift Φ_{DP} with a typical

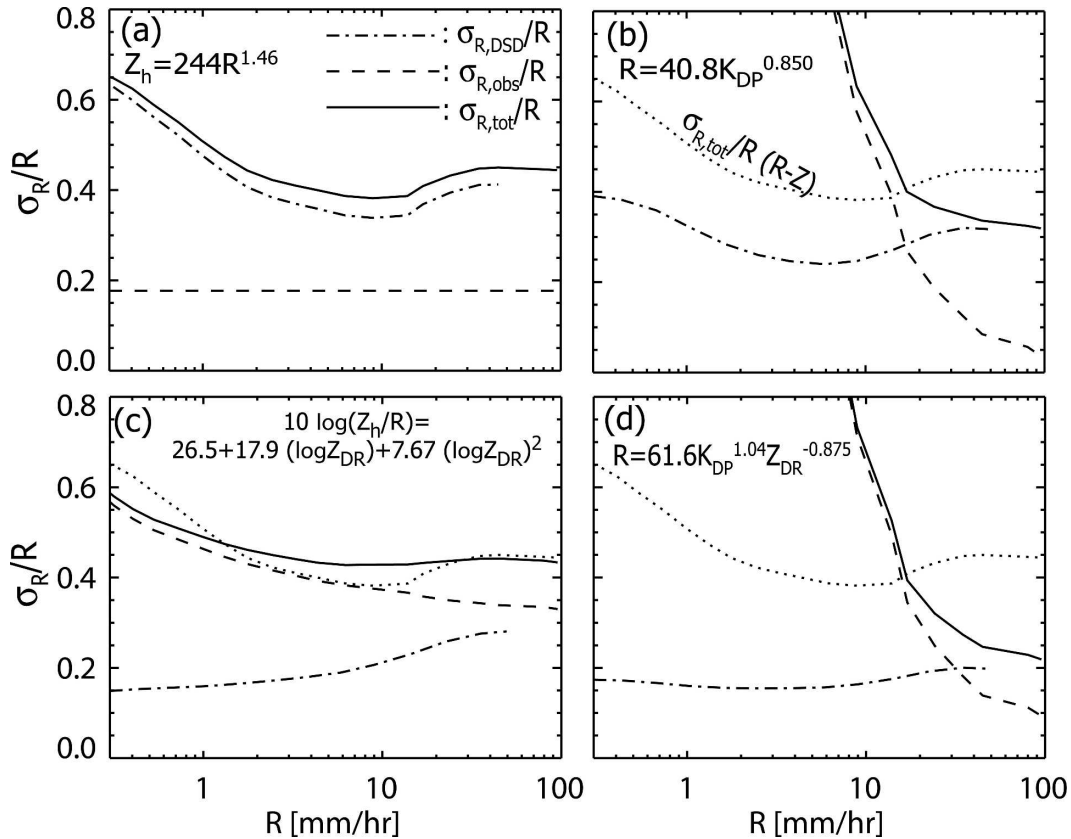


FIG. 5. (a)–(d) Normalized standard deviation in R for the indicated relationships resulting from the DSD variability ($\sigma_{R,DSD}/R$) and measurement noise ($\sigma_{R,obs}/R$). The total error ($\sigma_{R,tot}/R$), which is a combination of $\sigma_{R,DSD}/R$ and $\sigma_{R,obs}/R$, is indicated by the solid line. For comparison, the total error from the conventional $R - Z_h$ relationship in (a) is shown in all figures as a dotted line.

150-m range spacing, the measurement noise of $0.11^\circ \text{ km}^{-1}$ is expected in K_{DP} over a path of 6 km. They also reported that the typical accuracy of Z_h and Z_{DR} is about 1 and 0.2 dB, respectively. Ryzhkov and Zrnic (1995) also obtained the assumed measurement noise from the Cimarron radar with 64 sample pairs at 150-m range resolution and with a 4-km range smoothing. The σ_{Z_h} can be theoretically smaller than 1 dB, but this value is more realistic when we consider the uncertainty in radar calibration. In the case of the McGill radar (6 rpm), the measurement noise is greater.

The uncertainty ($\sigma_{R,DSD}/R$, dash-dotted lines), resulting from the DSD variability, is derived for raw 1-min DSDs as a function of rainfall intensity in a way similar to those from Table 1 and Fig. 1. The expected total error ($\sigma_{R,tot}/R$, solid line), resulting from the combined effect of the DSD variability and measurement noise, is obtained from the following equation:

$$\sigma_{R,tot}/R = [(\sigma_{R,DSD}/R)^2 + (\sigma_{R,obs}/R)^2]^{1/2}. \quad (6)$$

Here $\sigma_{R,DSD}/R$ for heavy rain is not calculated because of the small number of data, so that $\sigma_{R,DSD}/R$ at $R = 40 \text{ mm h}^{-1}$ is used for greater rain intensities. As reported in section 3 and the literature, results show that the DSD variability is a dominant factor in the conventional $R - Z_h$ relationship while it is less important in estimating R with polarimetric parameters. The $\sigma_{R,DSD}/R$ with $R - Z_h$ (Fig. 5a) has a minimum at moderate rain intensity ($R = 7 \sim 10 \text{ mm h}^{-1}$). That with $R - K_{DP}$ (Fig. 5b) shows a similar trend, except for an overall reduction of $\sim 10\% - 25\%$. The reduction of the effect of the DSD variability is significant with the $R - (Z_h, Z_{DR})$ and $R - (K_{DP}, Z_{DR})$ relationships (Figs. 5c and 5d) being $\sigma_{R,DSD}/R < 20\%$ over the entire range of R with the latter. However, it is to be noted that these $\sigma_{R,DSD}/R$ include the DSD measurement noise of POSS. Thus, the actual $\sigma_{R,DSD}/R$ should be smaller than these values.

The effect of radar measurement noise on rain estimates with a $R - Z_h$ relationship is less than 20%; the DSD variability is the key factor in the total error. Al-

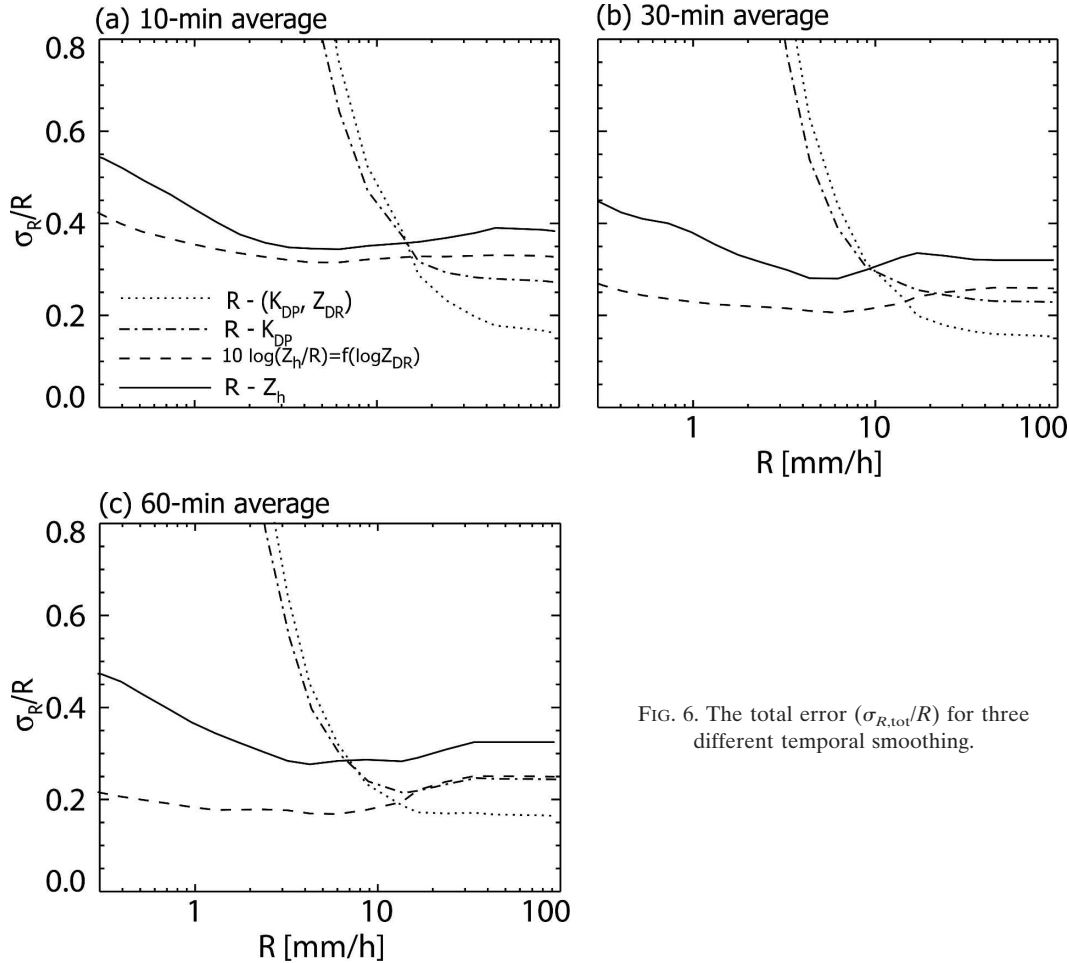


FIG. 6. The total error ($\sigma_{R,\text{tot}}/R$) for three different temporal smoothing.

though the effect of the DSD variability is significantly reduced with the R –(Z_h , Z_{DR}) in Fig. 5c, there is no significant reduction of the total error because of the larger measurement error in Z_{DR} . The conventional R – Z_h relationship performs better than R –(Z_h , Z_{DR}) at the range of $R = 2 \sim 20 \text{ mm h}^{-1}$. Hence, a reduction in the measurement error of Z_{DR} is necessary in order to achieve a better accuracy than that from the conventional R – Z_h relationship. This should be obtained by increasing the number of radar samples with averaging Z_{DR} over a longer range and time interval or with different scanning strategies. The uncertainty resulting from the measurement noise for the two relationships that include K_{DP} in Figs. 5b and 5d is dominant when $R < 14 \text{ mm h}^{-1}$. The total error becomes less than that from the R – Z_h relationship only when $R > 20 \text{ mm h}^{-1}$, thus limiting the advantage of K_{DP} to heavy rain. To extend this advantage to lower rain intensities, the increase of radar samples is essential as with Z_{DR} .

By applying the temporal smoothing, some of the DSD variability is filtered out and the DSD measure-

ment noise becomes insignificant. Radar measurement noise can also be reduced by temporal smoothing over the volume scans. Figure 6 shows the total error from the four formulas with different temporal smoothing. We assume that a radar volume scan is performed every 5 min. The return time of radar samples is every 5 min. This figure illustrates how polarimetric algorithms can improve on the conventional R – Z_h relationship by smoothing data obtained from successive scanning cycles. The R –(Z_h , Z_{DR}) relationship outperforms R – Z_h with 10-min smoothing over the entire range of rain intensity. The difference between the two algorithms increases with temporal smoothing, indicating that the reduction of radar measurement noise is more significant than that of the DSD variability. After an hour, the difference is about 10% at $R > 2 \text{ mm h}^{-1}$ (from about 30% to 20%). This is more a pronounced improvement than the results of Brandes et al. (2003) who showed an improvement from 47% for R – Z_h to 38% for R –(Z_h , Z_{DR}) (see their Table 3). As the temporal smoothing increases, the minimum rainfall intensity from which

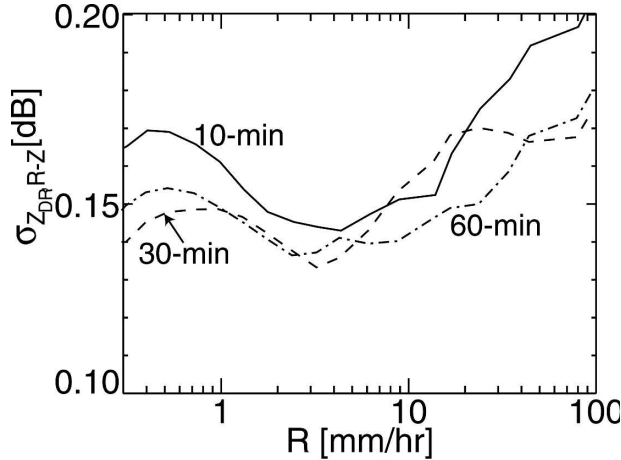


FIG. 7. The marginal measurement errors ($\sigma_{Z_{DR},R-Z}$) in Z_{DR} to have the same accuracy between $R-(Z_h, Z_{DR})$ and $R-Z_h$ algorithms at a given temporal smoothing.

the $R-K_{DP}$ or $R-(K_{DP}, Z_{DR})$ algorithms outperform $R-Z_h$ decreases from $R=14 \text{ mm h}^{-1}$ to $R=7 \text{ mm h}^{-1}$, suggesting that the smoothed K_{DP} also can improve the accuracy in moderate rain. The $R-(K_{DP}, Z_{DR})$ algorithm always performs best in heavy rain with a total error of less than 20%.

We can determine the standard deviation ($\sigma_{Z_{DR},R-Z}$) in Z_{DR} required in order that the $R-(Z_h, Z_{DR})$ and $R-Z_h$ algorithms yields the same accuracy for a given temporal smoothing. We call $\sigma_{Z_{DR},R-Z}$ the marginal measurement error. We derive $\sigma_{Z_{DR},R-Z}$ for which the solid and dashed lines in Fig. 6 cross over. We have fixed the measurement noise at $\sigma_{Z_h} = 1.0 \text{ dB}$ at instantaneous radar measurements (every 5 min) and have assumed that σ_{Z_h} decreases with temporal smoothing by $1/(\text{number of radar volume scans})^{0.5}$. Figure 7 shows $\sigma_{Z_{DR},R-Z}$ at three different temporal smoothings, and its average value is shown in Table 3. In general, there is no significant difference among the three smoothings. The variation of $\sigma_{Z_{DR},R-Z}$ with R is within the $\sim 0.13\text{--}0.2 \text{ dB}$ limits (Fig. 7). The average over the entire range of R is essentially unchanged at $\sim 0.15\text{--}0.16 \text{ dB}$ for the three smoothings selected (Table 3). This is the maximum noise level required to outperform the $R-Z_h$ relationship for the assumed volumetric scanning strategy. This unchanged noise level implies that instantaneous radar measurements could be noisier as long as they are temporally averaged. In general, this analysis suggests that, for the assumed scanning strategy, the $R-(Z_h, Z_{DR})$ algorithm can outperform the $R-Z_h$ with minimal smoothing when the measurement noise is below 0.2 dB. For a scanning strategy consisting of only a lowest PPI instead of a volumetric scan, the measurement noise could be larger because the return time of

TABLE 3. Standard deviation in ($Z_{DR,avg} - Z_{DR}$) resulting from the DSD variability ($\sigma_{Z_{DR},DSD}$), measurement noise ($\sigma_{Z_{DR},obs}$), and their combination ($\sigma_{Z_{DR},tot}$) at different temporal smoothings, where $Z_{DR,avg}$ indicates the average Z_{DR} as a function of Z_h ; $\sigma_{Z_{DR},DSD}$ is calculated from 5 yr of disdrometric data, and $\sigma_{Z_{DR},tot}$ is from data of five storms (26 h) collected by the McGill S-band operational polarimetric radar at a resolution of $1^\circ \times 1 \text{ km}$ and every 5 min. $\sigma_{Z_{DR},obs}$ is deduced from $\sigma_{Z_{DR},DSD}$ and $\sigma_{Z_{DR},tot}$ using (6), and $\sigma_{Z_{DR},R-Z}$ is the marginal measurement noise required to achieve the same accuracy in R with $R-Z_h$ and $R-(Z_h, Z_{DR})$ (see Fig. 7).

	$\sigma_{Z_{DR},DSD}$ (dB)	$\sigma_{Z_{DR},tot}$ (dB)	$\sigma_{Z_{DR},obs}$ (dB)	$\sigma_{Z_{DR},R-Z}$ (dB)
No averaging	0.22	0.35	0.27	0.16
10-min averaging	0.20	0.30	0.22	0.16
30-min averaging	0.19	0.26	0.18	0.15
60-min averaging	0.19	0.23	0.13	0.15

radar measurements is shorter. For example, for a return time of 1 min, the measurement noise could be as much as 0.5 dB by assuming that $\sigma_{Z_{DR}}$ decreases with temporal smoothing by $1/(\text{number of radar measurements})^{0.5}$.

c. Measurement noise with the McGill S-band polarimetric radar

For meteorological purposes, fast scanning ($\geq 3 \text{ rpm}$) is essential in order to increase the effectiveness of severe weather surveillance with data that are frequently updated. Hence, the dwelling time for each pixel (i.e., $1^\circ \times 1 \text{ km}$) is relatively short and the number of pulses is small. With the McGill S-band operational polarimetric radar (6 rpm), the number of independent samples is less than 20 at the resolution of $1^\circ \times 1 \text{ km}$. However, the results of Figs. 5 and 6 are based on assumptions adequate for a slow scanning radar ($\sim 1 \text{ rpm}$), where the number of the independent sample is much larger. Hence, we cannot expect the same quality of data from the McGill radar that require a fast scanning rate ($\geq 3 \text{ rpm}$). For example, $\sigma_{Z_h} = 1.2$ and 0.7 dB with 20 and 100 independent samples, respectively (Smith 1964). Therefore, more temporal or spatial smoothing is needed in order to achieve the accuracies shown in Figs. 5 and 6, resulting into a degradation of the temporal or spatial resolution. The nonhomogeneity of the precipitation field should then also be considered as another source of uncertainty (Gorgucci et al. 2000). On the other hand, the simultaneous sampling of the horizontally (H) and vertically (V) polarized signals has less measurement uncertainty in polarimetric parameters than the nonsimultaneous sampling (i.e., switched H/V on transmit and copolar receive) (Gingras et al. 1997).

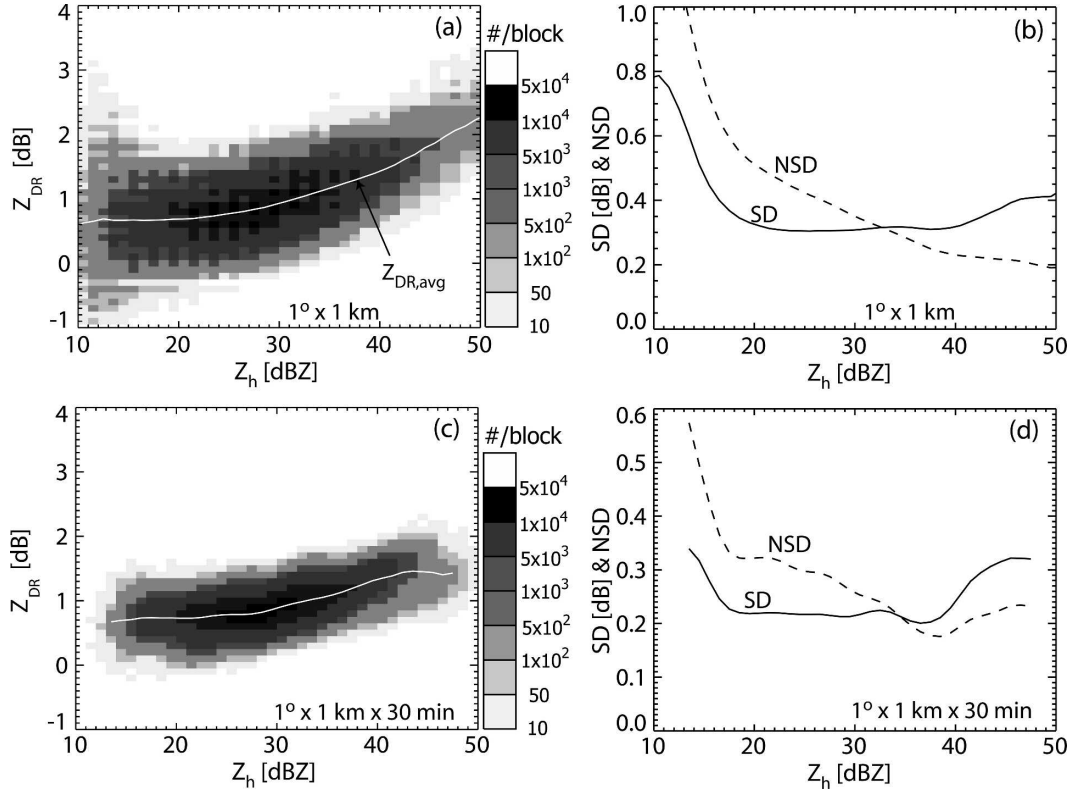


FIG. 8. (a) Frequency distribution of Z_{DR} as a function of Z_h from the operational S-band McGill polarimetric radar for five storms at a spatial resolution of $1^\circ \times 1$ km. The grayscale indicates number of data points. The solid line indicates the average of Z_{DR} . (b) SD and NSD with respect to the average of Z_{DR} . (c), (d) Same as in (a) and (b), except for the smoothing of Z_h and Z_{DR} at 30 min.

Consequently, the simultaneous sampling may be a better solution for the fast scanning radar, in terms of less degradation of the temporal or spatial resolution. The polarimetric Next-Generation Weather Radar (NEXRAD) prototype utilizes the simultaneous sampling (Doviak et al. 2000). McGill implementation of polarimetry is based on transmission at slant polarization and simultaneous reception of separated channels for H and V.

Figure 8 shows the frequency distribution, SD, and NSD of measured Z_{DR} as a function of measured Z_h from the McGill S-band operational polarimetric radar that uses the simultaneous sampling method. Polarimetric parameters are first obtained at a resolution of $1^\circ \times 1$ km every 5 min (Figs. 8a and 8b), which is then smoothed to $1^\circ \times 1$ km by 30 min (Figs. 8c and 8d). The detailed distributions of $(Z_{DR,avg} - Z_{DR})$ are shown in appendix C. The diagram illustrates all the variability ($\sigma_{Z_{DR,tot}}$) resulting from the measurement noise and the DSD variability. The SD and NSD statistics at $1^\circ \times 1$ km are particularly larger than those from the DSD variability from disdrometric data (see Fig. 4), indicating that the measurement noise with a scanning radar is

more important than the DSD variability. The distribution is narrowed by temporal smoothing at $1^\circ \times 1$ km by 30 min, confining SD within 0.2–0.3 dB throughout most of the range of Z_h . However, SD is still larger than that from the DSD variability after applying the temporal smoothing of 30 min (Fig. 4d).

We attempt to quantify the measurement noise ($\sigma_{Z_{DR,obs}}$) in Z_{DR} by comparing the DSD variability ($\sigma_{Z_{DR,DSD}}$) and the total variability ($\sigma_{Z_{DR,tot}}$); $\sigma_{Z_{DR,DSD}}$ is derived from disdrometric data with different temporal smoothings (1, 10, 30, 60 min) as in Fig. 4, and $\sigma_{Z_{DR,tot}}$ is also obtained for four temporal resolutions from the radar measurements as in Fig. 8. Both $\sigma_{Z_{DR,DSD}}$ and $\sigma_{Z_{DR,tot}}$ are derived over $20 \text{ dBZ} < Z_h < 50 \text{ dBZ}$. Then, the measurement noise $\sigma_{Z_{DR,obs}}$ is calculated from $\sigma_{Z_{DR,DSD}}$ and $\sigma_{Z_{DR,tot}}$ using (6). The results are shown in Table 3 for the four kinds of DSD variability (or temporal smoothing). If we accept the time-space analogy, the standard deviation resulting from the physical variability of DSD should be between 0.22 (1-min-averaged DSDs) and 0.19 (60-min-averaged DSDs) dB, depending on the temporal smoothing. The $\sigma_{Z_{DR,obs}}$ significantly decreases with temporal smooth-

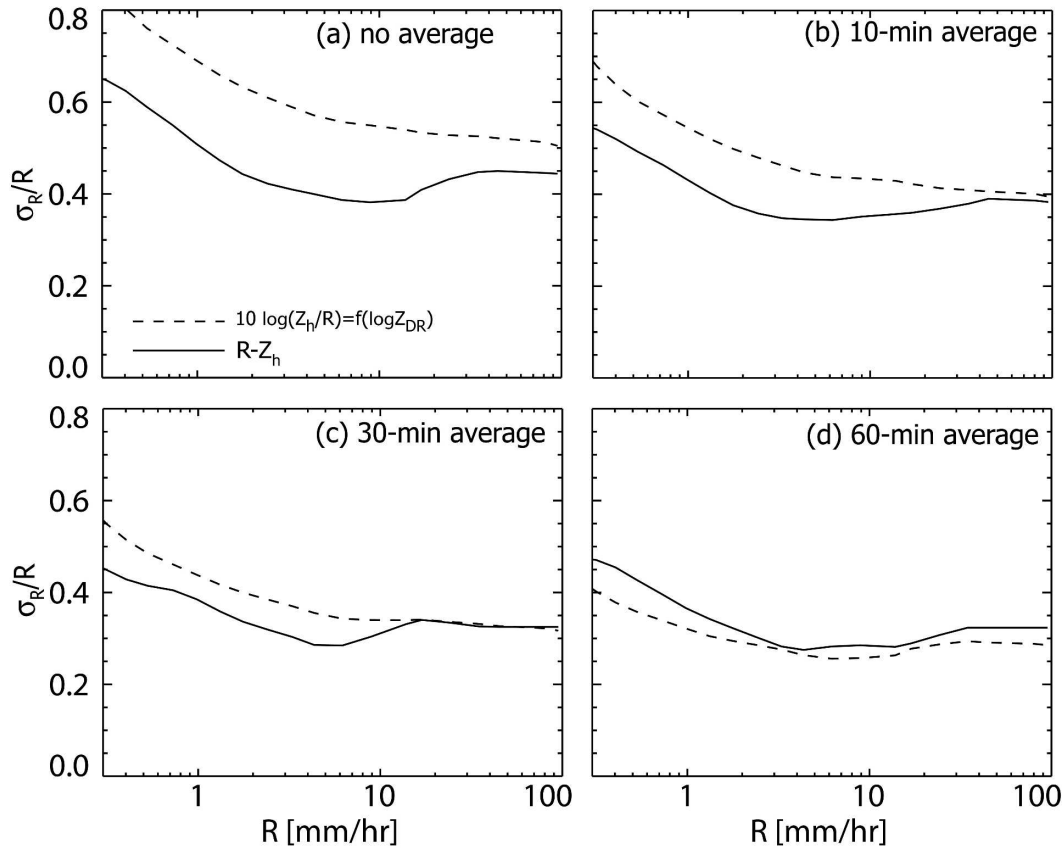


FIG. 9. Same as in Fig. 6, except for the derived measurement noise from the McGill S-band polarimetric radar shown in Table 3.

ing, but this reduction is less than that predicted by $1/(\text{number of radar volume scans})^{0.5}$. After smoothing over 30 min, $\sigma_{Z_{DR,obs}}$ ($=0.18$ dB) is less than $\sigma_{Z_{DR,DSD}}$ ($=0.19$ dB) but still is larger than the marginal measurement noise $\sigma_{Z_{DR,R-Z}}$ ($=0.15$ dB). Averaging over 1 h is required for the McGill S-band radar in order to reach the condition, $\sigma_{Z_{DR,obs}} < \sigma_{Z_{DR,R-Z}}$, which would enable the $R-(Z_h, Z_{DR})$ to outperform the conventional $R - Z_h$ relationship.

An analysis similar to Fig. 5 is performed with $\sigma_{Z_{DR,obs}}$ in Table 3 and with $\sigma_{Z_h} = 1.0$ dB. The total errors are only shown for the $R-Z_h$ and $R-(Z_h, Z_{DR})$ algorithms (see Fig. 9). The accuracy of $R-(Z_h, Z_{DR})$ is worse than that of $R - Z_h$ up to 30-min smoothing. The $R-(Z_h, Z_{DR})$ algorithm outperforms the $R - Z_h$ algorithm only after applying a 1-h smoothing. This poor performance of $R-(Z_h, Z_{DR})$ is due to the small number of samples that can be collected with the McGill S-band radar at the fast scan rate of 6 rpm. With a scan rate of 3 rpm, $\sigma_{Z_{DR,obs}}$ should be less than $\sigma_{Z_{DR,R-Z}}$ with only a 30-min smoothing and the $R-(Z_h, Z_{DR})$ algorithm should be more skillful than $R - Z_h$. This supports the recent

analysis by Ryzhkov et al. (2005) who demonstrate the superiority of $R-(Z_h, Z_{DR})$ for hourly rain accumulations with a volumetric scan at a scan rate of 3 rpm.

We should raise the question of the representativeness of the DSD variability. The calculated $\sigma_{Z_{DR,DSD}}$ is from 5 yr of disdrometric data whereas the radar data include the DSD variability for only five storms. Hence, $\sigma_{Z_{DR,DSD}}$ for these five storms is likely less than the value shown in the table because the DSD variability from the five storms may not include all variability included in the 5-yr disdrometric dataset. Thus, we can expect even larger $\sigma_{Z_{DR,obs}}$. Therefore, the temporal smoothing at an hour should be taken as a minimum requirement for obtaining improved rain estimates from the McGill S-band operational polarimetric radar at the current scanning strategy.

6. Conclusions

Five years of disdrometric data has been obtained with Precipitation Occurrence Sensing System (POSS).

Because of the large sampling volume of POSS (three orders of magnitude larger than the traditional disdrometer), the sampling Poisson noise is a second-order problem and larger drops are well detected (appendix A). Hence, the data are suitable for quantification of the DSD variability that is encountered with radar measurements. Twenty-six hours of radar data for five storms are obtained from the McGill S-band operational polarimetric radar collected with volumetric scans at a fast scanning speed of 6 rpm. Hence, we expect the measurement noise to be much higher than that from slow scanning radars [note that most of the radar data in the literature were obtained from a slow scanning speed of ~ 1 rpm except for Ryzhkov et al. (2005)]. Using both sets of data, sources of errors in rain measurement with polarimetric radar are explored in order to investigate their relative importance and the feasibility of a polarimetric technique for the estimation of R in the context of the McGill S-band operational radar. The sources of errors considered are the DSD variability, observational noise, and the variation of the relationships between R and polarimetric parameters. We have reached the following conclusions.

- 1) In agreement with published work, under ideal conditions the additional information from polarimetric radar drastically reduces the effect of the DSD variability in the estimation of R (Fig. 1 and Table 1). The form of the $10 \log(Z_h/R) = f(\log Z_{DR})$ relationship shows the best accuracy in light and moderate rain while $R = aK_{DP}^b Z_{DR}^c$ or $R = dZ_h^e K_{DP}^f$ relationships perform better with heavy rain. However, the $R = aK_{DP}^b Z_{DR}^c$ relationship is preferred with heavy rain because the reduction of the DSD variability with $R = dZ_h^e K_{DP}^f$ is very sensitive to the choice among the various drop deformation formulas given in the literature.
- 2) The relationships in the literature that are derived from the DSD model and measured DSDs differ from those derived from our disdrometric dataset (Fig. 2). Use of these relationships for the data in Montreal region results in a bias ($\sim 10\%$ – 20%) and significant random errors resulting from the DSD variability (Fig. 3). These results illustrate a systematic variation of these relationships in different climate regimes. This could be explained by the fact that the polarimetric relationships cannot account for all the DSD variability. Thus, the optimization of these relationships in a local environment is essential.
- 3) For the dataset observed in Montreal region, the standard deviation of Z_{DR} resulting from the DSD

variability ($\sigma_{Z_{DR},DSD}$) is derived as a function of Z_h and temporal smoothing. Here, $\sigma_{Z_{DR},DSD}$ varies from 0.22 dB for 1-min DSDs to 0.19 dB for 60-min average DSDs. These values should be considered as the limiting level of measurement noise of Z_{DR} needed to improve rain estimation with polarimetric parameters.

- 4) By assuming measurement noises of $\sigma_{Z_h,obs} = 1$ dB, $\sigma_{Z_{DR},obs} = 0.17$ dB, and $\sigma_{K_{DP},obs} = 0.11^\circ \text{ km}^{-1}$ that are expected from a slow scanning radar (~ 1 rpm) with range smoothing over a 4-km pathlength, the combined effect of the DSD variability and of measurement errors in the estimation of R is investigated for various rain estimation relationships (Figs. 5–6). The accuracy of $10 \log(Z_h/R) = f(\log Z_{DR})$ is comparable with the conventional $R - Z_h$ relationship for instantaneous radar measurements, the latter being $\sim 40\%$ – 65% . However, with minimal smoothing (~ 10 min or two radar scans), the $10 \log(Z_h/R) = f(\log Z_{DR})$ algorithm outperforms $R - Z_h$, confirming the advantage of polarimetric rain estimation. The accuracy of $R - Z_h$ is reduced to $\sim 35\%$ – 55% at this temporal scale. When K_{DP} is included in the relationship, the error in R is less than that of $R - Z_h$ only when $R > 7 \text{ mm h}^{-1}$ for an hourly accumulation. This analysis also leads to the marginal measurement noise ($\sigma_{Z_{DR},R-Z}$) of ~ 0.15 – 0.16 dB at which the $R - Z_h$ and $10 \log(Z_h/R) = f(\log Z_{DR})$ algorithms are comparable.
- 5) The measurement noise of the McGill S-band fast scanning operational radar is quantified at four temporal resolutions by comparing the standard deviation of Z_{DR} from radar observations with that resulting from the effect of the DSD variability (Fig. 8 and Table 3). The measurement noise decreases from 0.27 dB for instantaneous measurements to 0.13 dB for data smoothed over 60 min. The form of $10 \log(Z_h/R) = f(\log Z_{DR})$ can improve only hourly accumulations for the McGill S-band radar and possibly 30-min accumulations for the polarimetric NEXRAD prototype.

We have explored several sources for the uncertainty in R estimation with polarimetric parameters and quantified the expected errors. None of them can be neglected. In addition, as in conventional approach, the range effect resulting from radar beam broadening and the increases of measurement height is a significant factor that degrades the accuracy in R . Therefore, careful consideration on these sources is recommended before applying a polarimetric technique.

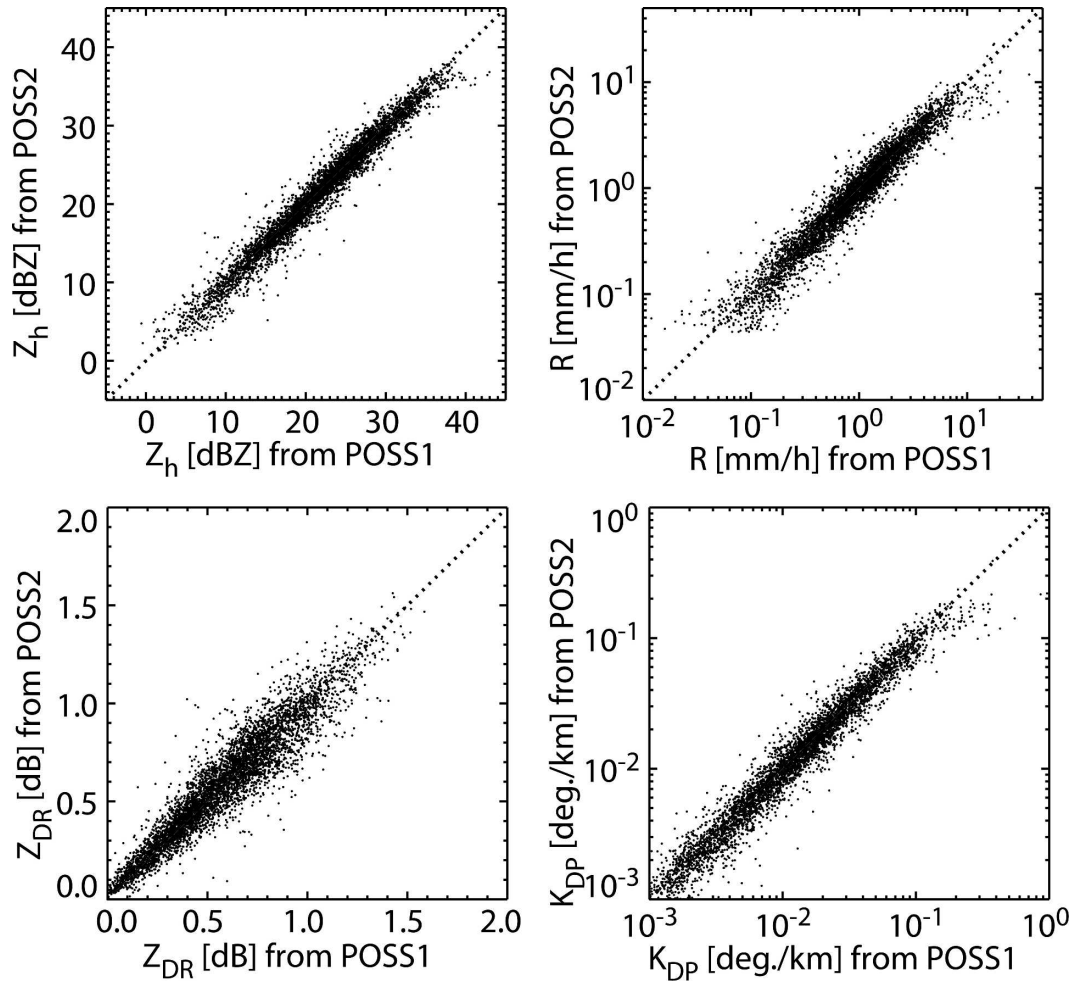


FIG. A1. Scatterplots of polarimetric parameters derived from 1-min-averaged DSD measurements with the two collocated POSSs.

Last but not least, we should point out that our simulation of radar measurements from DSDs implies a resolution volume that is smaller than the typical operational radar measurement volume. We have tried to compensate for the discrepancy by taking averages and considering long-term observations, but the problem of representativeness may still partially be present.

Acknowledgments. This work was partially supported by a grant from the Canadian Foundation for Climate and Atmospheric Sciences. The author is indebted to Professor I. Zawadzki for his guidance with intuitive comments and to Dr. Aldo Bellon for numerous constructive comments and for editing this manuscript. Numerous discussions on polarimetric data with Alamelu Kilambi at J. S. Marshall Radar Observatory have also been helpful.

APPENDIX A

Uncertainties in POSS Measurements

a. Comparison of two collocated POSSs

POSS measures Doppler spectra near the ground and converts them into DSDs. This conversion procedure and the effect of winds have been tested by Sheppard (1990) and Sheppard and Joe (1994). In addition, we have eliminated $N(D_i)$ when the total number of drops is less than 10 [$N_{\text{tot}}(D_i) < 10$] for all of the data analysis to minimize the undersampling effect (Lee and Zawadzki 2005a). In this appendix, we quantify the instrumental uncertainties of POSS by comparing data measured from two collocated POSSs for a period of 13 rain days. This comparison quantifies the uncertainty resulting from the undersampling and DSD retrieval algo-

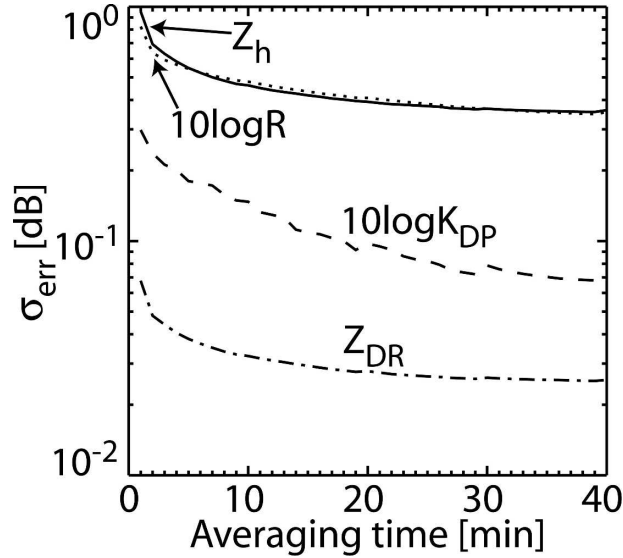


FIG. A2. Measurement errors of polarimetric parameters resulting from instrumental noise in the POSSs.

rithm. Polarimetric parameters are calculated from DSDs with a scattering model. The scatterplots of Z_h , R , Z_{DR} , and K_{DP} (Fig. A1) show a good agreement between the two POSSs. Each point is derived from 1-min DSDs and no filtering is applied. The small scatter is due to the DSD measurement errors of the two POSSs and to time mismatches (less than a minute) between them. In addition, their spatial distance also contributes to the scatter. By assuming that the standard deviation of measurement error distributions (σ_{err}) in the two POSSs are identical and both errors are uncorrelated, we have calculated σ_{err} in a way similar to that of Eq. (6). Because the two POSSs obtain DSDs with the same principle and are collocated, these assumptions should be valid. A similar calculation is performed with the temporal smoothing of DSDs up to 40 min. Results from raw measurements (averaging size = 1) show that $\sigma_{err,Z_h} = 0.96$ dB, $\sigma_{err,Z_{DR}} = 0.068$ dB, $\sigma_{err,10 \log R} = 0.82$ dB, and $\sigma_{err,10 \log K_{DP}} = 0.30$ dB (see Fig. A2). However, the actual measurement noise should be smaller than the calculated σ_{err} because of the time mismatches and spatial distance. The errors rapidly reduce with an initial 10-min averaging time (about 10% for R and Z_h , 3% for K_{DP} , and 1% for Z_{DR}). A further averaging does not reduce them dramatically except for $\sigma_{err,10 \log K_{DP}}$. In general, these results suggest that the measurements errors in POSS measurements resulting from the undersampling and retrieval algorithm can be neglected after 10-min averaging.

b. Comparison of collocated POSS and JWD

We have stated that the POSS measures bigger drops effectively because of the large sampling volume. This is evident in Figs. 6–9 of Sheppard and Joe (1994) for a limited number of DSDs. The comparison of collocated POSS and JWD is shown in Fig. A3 for over 4000 1-min-averaged DSDs measured for eight rain events in Montreal. Both R and Z are calculated at the range $D \geq 0.8$ mm in both JWD and POSS to avoid the improper dead correction and wind effects of JWD. No clear bias is present in R , whereas Z shows a systematic bias when $Z > 25$ dBZ. That is, the JWD underestimates Z . This can be explained by the difference in the sampling volumes of the two instruments. Because the sampling volume of POSS is three orders of magnitude larger than that of JWD, bigger drops are effectively well measured as shown in Fig. A3c.

The average DSDs from both instruments for the entire period are calculated by including all zero drop bins [$N(D) = 0 \text{ m}^{-3} \text{ mm}^{-1}$]. An exclusion of zero drop bins would have provided a positive bias in average DSDs. This bias is more noticeable for a disdrometer that has a small sampling volume. In this way, the average of integral parameters of DSDs is the same as those derived from the average DSD [see Eqs. (1) and (2) of Lee and Zawadzki (2005a)]. The average DSDs of the entire DSDs are almost identical when $0.9 \leq D \leq 2.0$ mm. (Note that the difference for $D < 0.9$ mm is caused by the inaccurate dead correction and wind effects of JWD.) However, when $D > 2.0$ mm, the JWD systematically underestimates. In summary, this figure illustrates the importance of a large sampling volume for properly detecting bigger drops.

APPENDIX B

Effects of SIFT on the Multiparameter Relationships

Lee and Zawadzki (2005a) used the sequential intensity filtering technique (SIFT) as a way of reducing instrumental and observational noises in disdrometric measurements, thus enabling real datasets to reveal the underlying microphysics. They show that SIFT provides a stable R – Z relationship that is independent of averaging time. As shown in section 5c, the polarimetric parameters from the McGill S-band radar have a large measurement noise that should be eliminated before transforming the parameters into R . Because most multiparameter relationships are nonlinear, it is crucial to eliminate noise before transforming the parameters into R . SIFT reduces the fluctuations of polarimetric parameters within a narrow interval of reflectivity.

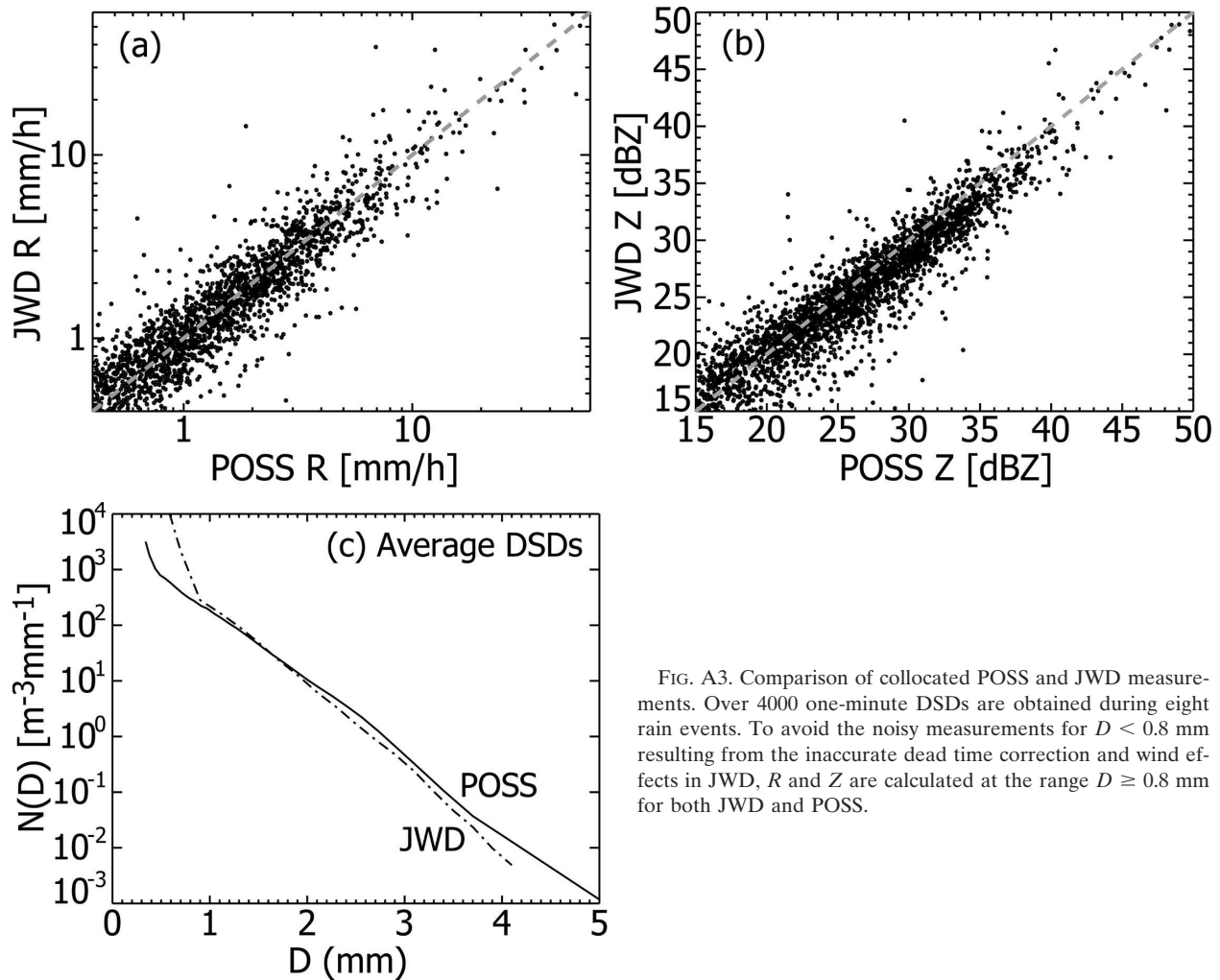


FIG. A3. Comparison of collocated POSS and JWD measurements. Over 4000 one-minute DSDs are obtained during eight rain events. To avoid the noisy measurements for $D < 0.8$ mm resulting from the inaccurate dead time correction and wind effects in JWD, R and Z are calculated at the range $D \geq 0.8$ mm for both JWD and POSS.

When different microphysical processes are included in a SIFT window, some physical variability is also filtered out. However, we are confident that SIFT mainly reduces the physical variability that is related to the systematic change of the generic shape of DSDs within a window of SIFT. We reach this conclusion from the collapse of all measured DSDs into a well-defined double-moment normalized DSD after applying SIFT (not shown in here). Therefore, following SIFT, most discernible DSDs can be described by the change in the intercept and slope parameters (i.e., the characteristic number density and diameter or two moments of DSDs; Lee et al. 2004) that are closely related to polarimetric parameters. Nevertheless, SIFT also improves the accuracy of R with polarimetric parameters although this improvement is more pronounced in a single parameter (R - Z_h and R - K_{DP} ; see Table 1). An error analysis shows that SIFT and 30-min-averaged DSDs yields comparable accuracy in R (see Figs. 2b and

4 of Lee and Zawadzki 2005b). However, we need to identify a proper time scale for SIFT. In this paper, we suggest SIFT as a way of filtering out noisy polarimetric parameters from the McGill S-band radar. While some physical variability is undesirably reduced, it can be minimized by combining data in space and time. We can confine the window size of SIFT into a space-time domain (i.e., $10^\circ \times 10 \text{ km} \times 10 \text{ min}$) where the change of microphysics should be minimal and the number of data should be sufficient to apply SIFT.

We need to ensure that SIFT can provide a stable relationship between R and the polarimetric parameters as is the case with the R - Z relationship. For the climatological DSD dataset used in Table 1, we have applied SIFT with an averaging time from 1 to 30 min while fixing the window size ($W = 1 \text{ h}$). DSDs within an hour are sorted with increasing Z and then the moving average of ~ 1 -30 min is applied. Multiparameter relationships are then derived at each averaging time and

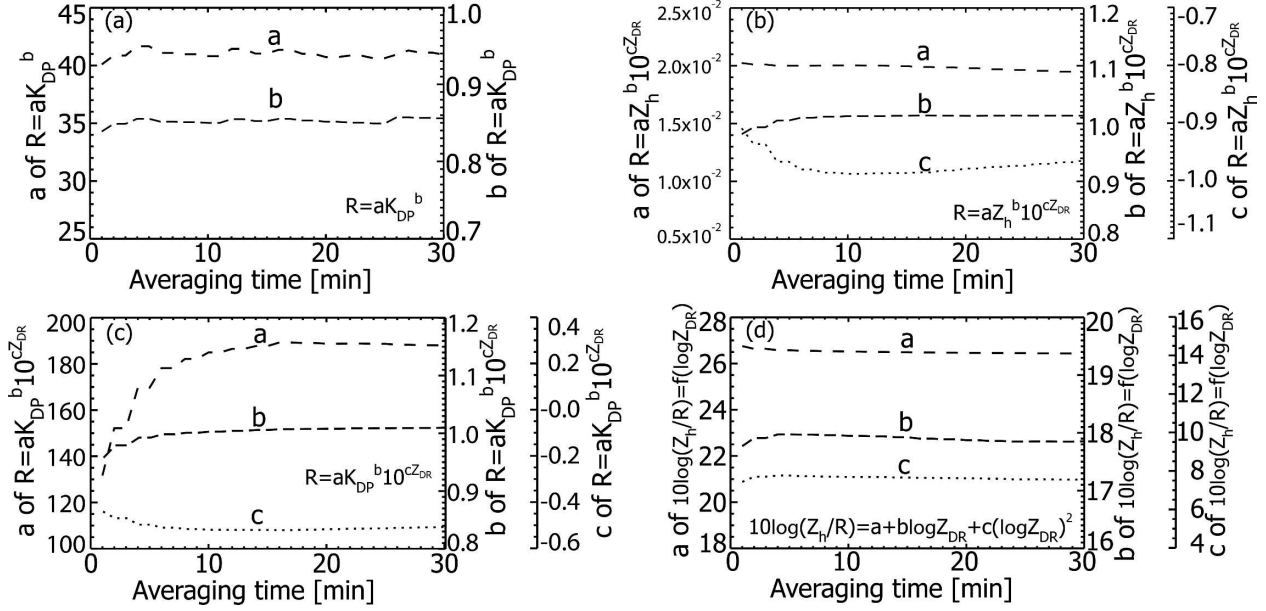


FIG. B1. Multiparameter relationships after applying SIFT. The window size of SIFT is fixed at an hour and the averaging size varies from 1 to 30 min. The relationship is nearly independent of the averaging size for an averaging time > 10 min.

are shown in Fig. B1. This diagram illustrates how well SIFT derives a stable relationship that is independent of the averaging time. There is no significant change of $R = aK_{DP}^b$ and $10 \log(Z_h/R) = f(\log Z_{DR})$ for the entire range of the averaging time. A slight change is noticed in $R = aZ_h^b 10^{cZ_{DR}}$ and $R = aK_{DP}^b 10^{cZ_{DR}}$ when the averaging size < 10 min. In general, the relationships become stable after applying SIFT with an averaging time of 10 min, emphasizing the effectiveness of SIFT in stabilizing the relationships. When applying SIFT with actual radar measurements, the averaging size can be any minimum value that depends on the level of noise. The averaging of polarimetric parameters within a narrow interval of Z followed by a transformation into R using the relationships (Fig. B1) should increase the accuracy in R when using the noisy measurements from the McGill S-band polarimetric radar.

APPENDIX C

Distributions of the Difference between $Z_{DR,avg}$ and Z_{DR}

In Figs. 4 and 8, the distributions of Z_{DR} and the standard deviations of $(Z_{DR,avg} - Z_{DR})$ were shown as a function of Z_h . Then, $\sigma_{(Z_{DR,avg} - Z_{DR}),DSD}$ and $\sigma_{(Z_{DR,avg} - Z_{DR}),tot}$ were derived to quantify the effect of the DSD variability and of measurement noise. In this appendix, we show whether $\sigma_{(Z_{DR,avg} - Z_{DR}),DSD}$ or $\sigma_{(Z_{DR,avg} - Z_{DR}),tot}$ is statistically meaningful. Figure C1

shows the frequency distributions of $(Z_{DR,avg} - Z_{DR})$ for DSDs and radar observations with different temporal smoothing. Note that the values of $Z_{DR,avg}$ are a function of Z_h (solid lines in Figs. 4a, 4c, 8a, and 8c). The standard deviations of these distributions are the same values seen in Table 3. The distributions are almost symmetric with a bias of zero. These distributions are compared with a Gaussian distribution (dashed lines) of the same standard deviation and mean. Results show that the measured distributions follow well the Gaussian distribution. Thus, we can consider that the derived standard deviation from these distributions has a statistically similar meaning as the Gaussian distribution.

The distributions are the outcome of the measurement noises with POSS or radar and of the physical variability. Thus, the narrower distributions with temporal smoothing are due to the reduction of both of these causes. Because the measurement noise with POSS becomes insignificant with smoothing over 10 min (see appendix A), the distribution with $\sigma_{Z_{DR,avg} - Z_{DR},DSD} = 0.19$ dB is due to the physical variability. The reduction of the standard deviation with temporal smoothing is more noticeable in radar measurements, indicating its importance to reduce its measurement noise. The distributions from radar measurements are wider than their counterparts from DSDs, particularly Figs. C1a and C1c. The difference of corresponding two distributions can be explained mostly by the radar measurement noise because we assume the

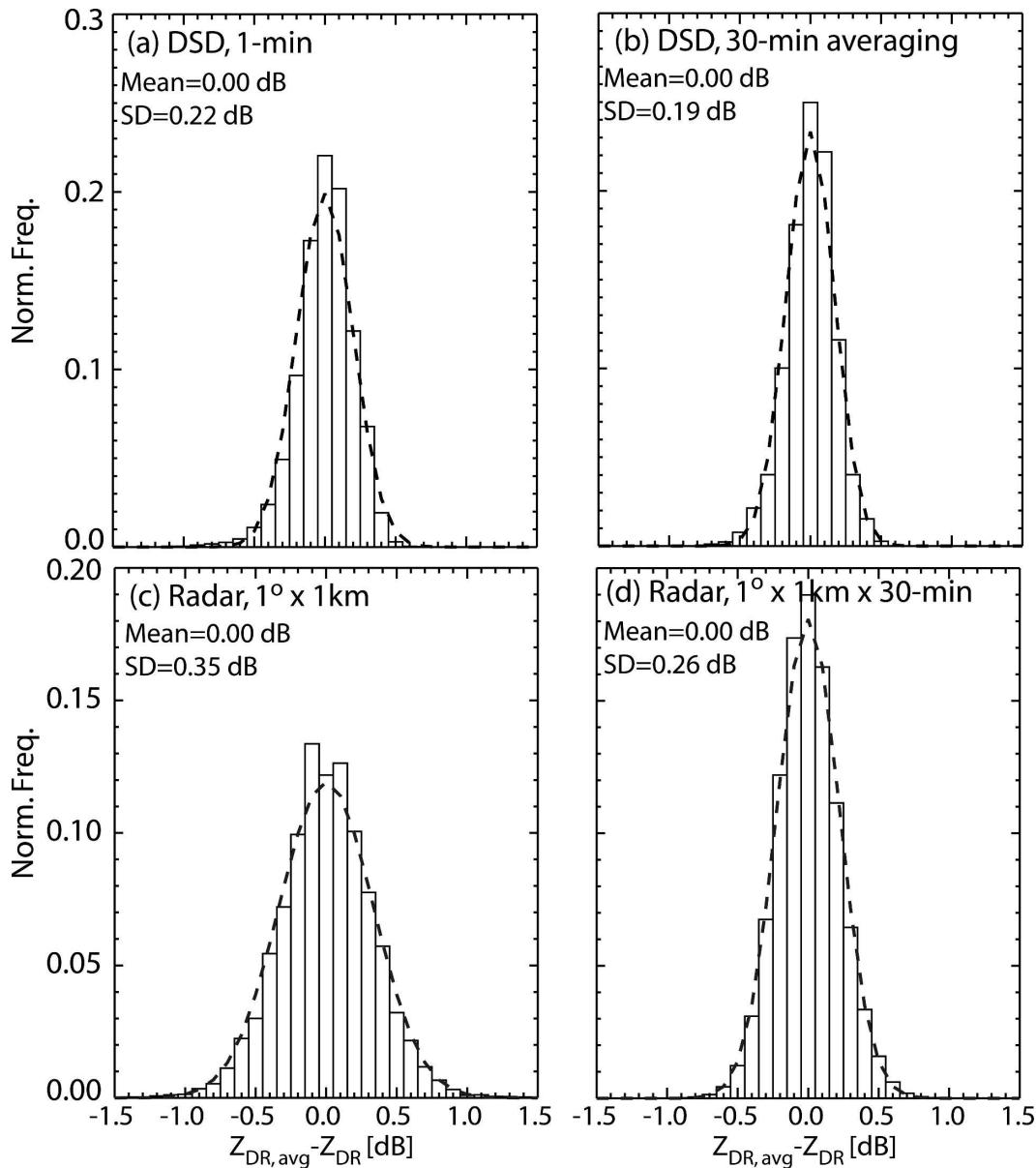


FIG. C1. Distributions of $(Z_{DR,avg} - Z_{DR})$ for DSDs and radar measurements with different temporal smoothing. The dashed curve indicates a Gaussian distribution that has the same SD and mean as the actual distribution.

DSD variability seen by POSS and radar is identical with 30-min smoothing. In addition, the set of DSD data includes the physical variability more than that of the radar measurement resulting from the difference in the number of cases. Thus, the actual $\sigma_{(Z_{DR,avg} - Z_{DR}),obs}$ could be larger than the derived value.

REFERENCES

- Andsager, K., K. Beard, and N. F. Laird, 1999: Laboratory measurements of axis ratios for large raindrops. *J. Atmos. Sci.*, **56**, 2673–2683.
- Auf der Maur, A. N., 2001: Statistical tools for drop size distributions: Moments and generalized gamma. *J. Atmos. Sci.*, **58**, 407–418.
- Balakrishnan, N., D. S. Zrnic, J. Goldhirsh, and J. Rowland, 1989: Comparison of simulated rain rates from disdrometer data employing polarimetric radar algorithms. *J. Atmos. Oceanic Technol.*, **6**, 476–486.
- Battan, L. J., 1973: *Radar Observation of the Atmosphere*. University of Chicago Press, 324 pp.
- Bevington, P. R., 1969: *Data Reduction and Error Analysis for the Physical Sciences*. McGraw-Hill, 336 pp.
- Brandes, E. A., G. Zhang, and J. Vivekanandan, 2003: An evalu-

- ation of a drop distribution-based polarimetric radar rainfall estimator. *J. Appl. Meteor.*, **42**, 652–660.
- Bringi, V. N., V. Chandrasekar, N. Balakrishnan, and D. S. Zrnice, 1990: An examination of propagation effects in rainfall on radar measurements at microwave frequencies. *J. Atmos. Oceanic Technol.*, **7**, 829–840.
- , —, D. Zrnice, and C. W. Ulbrich, 2003: Comments on “The need to represent raindrop size spectra as normalized gamma distributions for the interpretation of polarization radar observations.” *J. Appl. Meteor.*, **42**, 1184–1189.
- Campos, E., and I. Zawadzki, 2000: Instrumental uncertainties in Z–R relations. *J. Appl. Meteor.*, **39**, 1088–1102.
- Chandrasekar, V., and V. N. Bringi, 1987: Simulation of radar reflectivity and surface measurements of rainfall. *J. Atmos. Oceanic Technol.*, **4**, 464–478.
- , and —, 1988: Error structure of multiparameter radar and surface measurements of rainfall. Part I: Differential reflectivity. *J. Atmos. Oceanic Technol.*, **5**, 783–795.
- , —, N. Balakrishnan, and D. S. Zrnice, 1990: Error structure of multiparameter radar and surface measurements of rainfall. Part III: Specific differential phase. *J. Atmos. Oceanic Technol.*, **7**, 621–629.
- , E. Gorgucci, and G. Scarchilli, 1993: Optimization of multiparameter radar estimates of rainfall. *J. Appl. Meteor.*, **32**, 1288–1293.
- Ciach, G. J., and W. F. Krajewski, 1999: Radar-rain gauge comparisons under observational uncertainties. *J. Appl. Meteor.*, **38**, 1519–1525.
- , M. L. Morrissey, and W. F. Krajewski, 2000: Conditional bias in radar rainfall estimation. *J. Appl. Meteor.*, **39**, 1941–1946.
- Doviak, R. J., and D. S. Zrnice, 1993: *Doppler Radar and Weather Observations*. Academic Press, 562 pp.
- , V. Bringi, A. Ryzhkov, A. Zahrai, and D. Zrnice, 2000: Considerations for polarimetric upgrades to operational WSR-88D radars. *J. Atmos. Oceanic Technol.*, **17**, 257–278.
- Gingras, Y., E. Torlaschi, and I. Zawadzki, 1997: A theoretical comparison between staggered and simultaneous H/V sampling in dual-polarization radar. Preprints, *28th Conf. on Radar Meteorology*, Austin, TX, Amer. Meteor. Soc., 23–24.
- Goddard, J. W., K. L. Morgan, A. J. Illingworth, and H. Sauvageot, 1995: Dual-wavelength polarization measurements in precipitation using the camera and Rabelais radars. Preprints, *27th Conf. on Radar Meteorology*, Vail, CO, Amer. Meteor. Soc., 196–198.
- Gorgucci, E., V. Chandrasekar, and G. Scarchilli, 1995: Radar and surface measurement of rainfall during CaPE: 26 July 1991 case study. *J. Appl. Meteor.*, **34**, 1570–1577.
- , G. Scarchilli, and V. Chandrasekar, 2000: Practical aspects of radar rainfall estimation using specific differential propagation phase. *J. Appl. Meteor.*, **39**, 945–955.
- , V. Chandrasekar, V. N. Bringi, and G. Scarchilli, 2002: Estimation of raindrop size distribution parameters from polarimetric radar measurements. *J. Atmos. Sci.*, **59**, 2373–2384.
- Green, A. W., 1975: An approximation for the shapes of large rain-drops. *J. Appl. Meteor.*, **14**, 1578–1583.
- Gunn, R., and G. D. Kinzer, 1949: The terminal velocity of fall for water droplets in stagnant air. *J. Meteor.*, **6**, 243–248.
- Illingworth, A. J., and T. M. Blackman, 2002: The need to represent raindrop size spectra as normalized gamma distributions for the interpretation of polarization radar observations. *J. Appl. Meteor.*, **41**, 286–297.
- Jameson, A. R., 1994: An alternative approach to estimate rainfall rate by radar using propagation differential phase shift. *J. Atmos. Oceanic Technol.*, **11**, 122–139.
- Joss, J., and I. Zawadzki, 1997: Raindrop size distribution again? Preprints, *28th Conf. on Radar Meteorology*, Austin, TX, Amer. Meteor. Soc., 326–327.
- Keenan, T. D., L. D. Carey, D. S. Zrnice, and P. T. May, 2001: Sensitivity of 5-cm wavelength polarimetric radar variables to raindrop axial ratio and drop size distribution. *J. Appl. Meteor.*, **40**, 526–545.
- Lee, G. W., 2003: Errors in rain measurement by radar: Effect of variability of drop size distributions. Ph.D. thesis, McGill University, 279 pp. [Available online at http://www.radar.mcgill.ca/~gwlee/PAPERS/THESIS_2003/thesis_gwlee_single.pdf.]
- , and I. Zawadzki, 2005a: Variability of drop size distributions: Noise and noise filtering in disdrometric data. *J. Appl. Meteor.*, **44**, 634–652.
- , and I. Zawadzki, 2005b: Variability of drop size distributions: Time-scale dependence of the variability and its effects on rain estimation. *J. Appl. Meteor.*, **44**, 241–255.
- , and I. Zawadzki, 2005c: Radar calibration by gage, disdrometer, and polarimetry: Theoretical limit caused by the variability of drop size distribution and application to fast scanning operational radar data. *J. Hydrol.*, in press.
- , —, W. Szymer, D. Sempere-Torres, and R. Uijlenhoet, 2004: A general approach to double-moment normalization of drop size distributions. *J. Appl. Meteor.*, **43**, 264–281.
- Liu, H. P., and V. Chandrasekar, 2000: Classification of hydrometeors based on polarimetric radar measurements: Development of fuzzy logic and neuro-fuzzy systems, and in situ verification. *J. Atmos. Oceanic Technol.*, **17**, 140–164.
- Marshall, J. S., and W. McK. Palmer, 1948: The distribution of raindrops with size. *J. Meteor.*, **5**, 165–166.
- Mirovsky, B. J., and Coauthors, 2004: An experimental study of small-scale variability of radar reflectivity using disdrometer observations. *J. Appl. Meteor.*, **43**, 106–118.
- Mishchenko, M. I., J. W. Hovenier, and L. D. Travis, 2000: *Light Scattering by Nonspherical Particles*. Academic Press, 690 pp.
- Montero-Martinez, G., and F. Garcia-Garcia, 2004: Multipeak raindrop spectra observations from convective showers in Mexico. Preprints, *14th Int. Conf. on Clouds and Precipitation*, Bologna, Italy, International Association of Meteorology and Atmospheric Sciences (IAMAS), 604–607.
- Pruppacher, H. R., and K. V. Beard, 1970: A wind tunnel investigation of the internal circulation and shape of water drops falling at terminal velocity in air. *Quart. J. Roy. Meteor. Soc.*, **96**, 247–256.
- Ryzhkov, A. V., and D. S. Zrnice, 1995: Comparison of dual-polarization radar estimators of rain. *J. Atmos. Oceanic Technol.*, **12**, 249–256.
- , and —, 1998: Discrimination between rain and snow with a polarimetric radar. *J. Appl. Meteor.*, **37**, 1228–1240.
- , S. E. Giangrande, and T. J. Schuur, 2005: Rainfall estimation with a polarimetric prototype of WSR-88D. *J. Appl. Meteor.*, **44**, 502–515.
- Sachidananda, M., and D. S. Zrnice, 1987: Rain rate estimates from differential polarization measurements. *J. Atmos. Oceanic Technol.*, **4**, 588–598.
- Salles, C., and J.-D. Creutin, 2003: Instrumental uncertainties in Z–R relationships and raindrop fall velocities. *J. Appl. Meteor.*, **42**, 279–290.

- Sauvageot, H., and J.-P. Lacaux, 1995: The shape of averaged drop size distributions. *J. Atmos. Sci.*, **52**, 1070–1083.
- Sekhon, R. S., and R. C. Srivastava, 1971: Doppler radar observations of drop-size distributions in a thunderstorm. *J. Atmos. Sci.*, **28**, 983–994.
- Seliga, T. A., and V. N. Bringi, 1976: Potential use of radar differential reflectivity measurements at orthogonal polarizations for measuring precipitation. *J. Appl. Meteor.*, **15**, 69–76.
- , K. Aydin, and H. Direskeneli, 1986: Disdrometer measurements during an intense rainfall events in central Illinois: Implications for differential reflectivity radar observations. *J. Climate Appl. Meteor.*, **25**, 835–846.
- Sheppard, B. E., 1990: Measurement of raindrop size distribution using a small Doppler radar. *J. Atmos. Oceanic Technol.*, **7**, 255–268.
- , 2006: Sampling errors in the measurement of rainfall parameters using the precipitation occurrence sensor system (POSS). *J. Atmos. Oceanic Technol.*, in press.
- , and P. I. Joe, 1994: Comparison of raindrop size distribution measurements by a Joss-Waldvogel disdrometer, a PMS 2DG spectrometer, and a POSS Doppler radar. *J. Atmos. Oceanic Technol.*, **11**, 874–887.
- Smith, P. L., 1964: Interpretation of the fluctuating echo from randomly distributed scatterers. Part 3. Stormy Weather Group, McGill University, Rep. MW-39, 70 pp.
- , L. Zhong, and J. Joss, 1993: A study of sampling-variability effects in raindrop size observations. *J. Appl. Meteor.*, **32**, 1259–1269.
- Testud, J., S. Oury, R. A. Black, P. Amayenc, and X. Dou, 2001: The concept of “normalized” distribution to describe raindrop spectra: A tool for cloud physics and cloud remote sensing. *J. Appl. Meteor.*, **40**, 1118–1140.
- Torlaschi, E., and I. Zawadzki, 2003: The effect of mean and differential attenuation on the precision and accuracy of the estimates of reflectivity and differential reflectivity. *J. Atmos. Oceanic Technol.*, **20**, 362–371.
- Uijlenhoet, R., 1999: *Parameterization of Rainfall Microstructure for Radar Meteorology and Hydrology*. Ph.D. dissertation, Wageningen University, 279 pp.
- , J. A. Smith, and M. Steiner, 2003: The microphysical structure of extreme precipitation as inferred from ground-based raindrop spectra. *J. Atmos. Sci.*, **60**, 1220–1238.
- Ulbrich, C. W., 1983: Natural variations in the analytical form of the raindrop size distribution. *J. Climate Appl. Meteor.*, **22**, 1764–1775.
- Vivekanandan, J., D. S. Zrnic, S. M. Ellis, R. Oye, A. V. Ryzhkov, and J. Straka, 1999: Cloud microphysics retrieval using S-band dual-polarization radar measurements. *Bull. Amer. Meteor. Soc.*, **80**, 381–388.
- Waldvogel, A., 1974: The N_0 jump of raindrop spectra. *J. Atmos. Sci.*, **31**, 1067–1078.
- Willis, P. T., 1984: Functional fits to some observed drop size distributions and parameterization of rain. *J. Atmos. Sci.*, **41**, 1648–1661.
- Zawadzki, I., and G. W. Lee, 2004: The physical causes of the variability of drop size distributions. Preprints, *14th Int. Conf. on Clouds and Precipitation*, Bologna, Italy, The International Association of Meteorology and Atmospheric Sciences (IAMAS), 698–701.
- , A. Bellon, C. Cote, and F. Fabry, 2001: Target identification by dual-polarization radar in an operational environment. Preprints, *30th Conf. on Radar Meteorology*, Munich, Germany, Amer. Meteor. Soc., 165–167.
- Zrnic, D. S., T. D. Keenan, L. D. Carey, and P. May, 2000: Sensitivity analysis of polarimetric variables at a 5-cm wavelength in rain. *J. Appl. Meteor.*, **39**, 1514–1526.